NUREG/CR-1840
R6, RB

A Numerical Model Pertaining to the Multiple Vortex Phenomenon

Final Report
May 1978 - April 1980

Manuscript Completed: November 1980
Date Published: January 1981

Prepared by
R. Rotunno*, D. K. Lilly

*Cooperative Institute for Research in the Environmental Sciences
University of Colorado
Boulder, CO 30303

National Center for Atmospheric Research
Boulder, CO 80303

Prepared for
Division of Reactor Safety Research
Office of Nuclear Regulatory Research
U.S. Nuclear Regulatory Commission
Washington, D.C. 20555
NRC FIN B6238
Under Contract No. NRC-04-78-247

ABSTRACT

A three dimensional numerical model has been constructed for study of the multiple vortex phenomena. It is found that highly asymmetric vortices form at the core boundary of the larger parent vortex for certain values of the swirl ratio, S and radial Reynolds number. The asymmetric vortices arise as an instability of the initially axisymmetric parent vortex. The peak velocity associated with the mature asymmetric vortices can be 20%-30% larger than that of the parent vortex. The asymmetric vortices assume the form of intertwining helicies of negative pitch angle (the streamlines of the parent vortex are helical with positive pitch angle). This and other features are in agreement with a relevant laboratory experiment.

CONTENTS

LIST OF FIGURES

LIST OF SYMBOLS

a - non-dimensional radius of a fictitious inner cylinder

c_i - imaginary phase speed

L - number of grid volumes in azimuthal direction

M - number of grid volumes in radial direction

N - number of grid volumes in vertical direction

P - pressure (dimensional, if primed)

r - radial coordinate

θ - azimuthal coordinate

z - vertical coordinate

u - radial velocity (dimensional, if primed)

v - azimuthal velocity (dimensional, if primed)

w - vertical velocity (dimensional, if primed)

ξ - radial vorticity

η - azimuthal vorticity

ζ - vertical vorticity

Γ - circulation = rxv

m - azimuthal wavenumber

k - vertical wavenumber

ν - eddy viscosity

t - time

τ - time step number ($t = \tau\Delta t$)

Δt - time step

Δr - radial grid size

Δz - vertical grid size

$r\Delta\theta$ - azimuthal grid size

t_s - spin-up time of rotating screen

ρ - fluid density

Re - radial Reynolds number

S - swirl ratio

R - domain radius

Q - volume flow rate through chamber $[L^3/T]$

K - parameter in partial slip formula

1.0 Introduction

It often occurs that tornadoes contain smaller subsidiary vortices which revolve about the tornado, which in turn, rotate in the same sense (see Fujita, 1970; Forbes, 1978). This phenomenon goes by various names ("suction vortices", "satellite vortices", and "secondary vortices"), however, for this work we follow Church et al. (1979) and refer to the multiple vortex phenomenon (MVP). So when we speak of the MVP we refer to that type of "suction vortex" which Fujita (1976) has termed the "orbiting vortex". That the MVP may be more than a minor detail of the tornadic flow is suggested by damage surveys which indicate the most intense destruction of life and property is associated with cycloidal paths which Fujita has termed "suction swaths". As with the tornado, very little is known about the internal circulation of the MVP. Photogrametric and ground survey data are inconclusive on such important questions as to i) what maximum wind speed is achieved by the tornado and ii) the relation between this and the MVP. MVs are clearly visible in photographs but it is extremely difficult to infer actual flow patterns.

Ward (1972) built a laboratory device intended to simulate tornadic flow. Among the facts which argue for the validity of Ward's model is the result that for certain values of the swirl ration (defined below) the single central vortex divides into two or more vortices. Until recently, the data from the Ward vortex chamber was, for the most part, from flow visualization techniques and surface pressure measurements. Church et al. (1979) have reported on the internal flow, however, as of this writing have not measured the three velocity components separately as a function of space and time.

All analytical and/or numerical models of tornadoes to date are axisymmetric i.e., with respect to a system of cylindrical coordinates, azimuthal variations are not allowed. Clearly, the physical system under discussion is essentially asymmetric. Simple analytical axisymmetric vortex models are of great utility for understanding some basic physical processes (see e.g., Lewellen, 1976) and provide a basic reference point for more complex numerical models which add certain refinements. However, for three-dimensional asymmetric vortices of the type discussed here even simple models are lacking. It is important to know how theoretical (based on axisymmetric models) estimates of the magnitude, location and duration of the maximum tornadic wind depend on the flow asymmetry. Further, one would like to know the flow field of an asymmetric vortex so as to ascertain the type and magnitude of stresses to be expected on structures.

The aim of this work is to ascertain the general effect these flow asymmetries may have on the tornadic flow field. The principal research tool used is a fully three-dimensional numerical model in cylindrical coordinates; the model is based on Ward's physical model of a mesocyclone upon which Ward based his laboratory device. This model and its relation to nature is detailed in the following section. Axisymmetric calculations and theory of axisymmetric swirling flows are discussed in Section 4. Section 5 contains a description of the numerical model. Section 6 contains the results of the model integrations, while interpretations are saved for Section 7.

Principal findings are:

i) MVs arise as an instability of an axisymmetric flow as hypothesized by Ward (1972). Unstable waves grow to finite amplitude and become the MV. As an unstable wave grows, angular momentum is transported inward by the wave and the inner core is spun-up. The flow is thus stabilized and the large amplitude structures persist.

ii) The present model exhibits good agreement with certain features of the laboratory model, viz. the MV pattern progresses at approximately the local rotation rate of the flow at low levels. The local tangential velocity of the MV can be 20-30% larger than the azimuthal average at the radius of v_{max}, thus suggesting that MVs should indeed cause more local damage as has been observed. (Further, the 3-D model with MVs again has local tangential velocities between 20-30% higher than an equivalent axisymmetric model which uses the same external parameters.)

iii) The actual distribution of flow velocity within a MV is quite asymmetric with large positive vertical and tangential velocities on one side with reduced (or in some cases negative) vertical and tangential velocities on the other. This distribution is reasonable and can be explained as a natural consequence of the distribution of vorticity in the initially (unstable) axisymmetric flow. Other details of the flow are discussed.

2.0 Physical Model

Brooks (1949) discovered the existence of a "wind and pressure system intermediate in size between the general parent low and the tornado funnel itself." The existence of a rotating updraft within severe storms was inferred by Browning (1964) from the hook-echo observed by radar.[2] The scale of the updraft diameter is typically O(5-12 km) (Browning, 1978) which is an order of magnitude larger than a typical tornado funnel (O(100 m)). The inflow layer which feeds the updraft is O(1-2 km) in depth. The updraft radius, R, divided by the inflow layer depth h is termed the aspect ratio, h/R. Ward (1972) realized that all laboratory experiments purporting to model tornadoes used aspect ratios which were much too small, while the present discussion indicates h/R should be O(1).

Ward's device is shown in Fig. 1a. This configuration is compared with dual-doppler radar data (Fig. 1b, Brandes, 1978) which indicate that Ward's original design is relevant. Referring to Fig. 1a we see there is a cylindrical chamber bounded above by a honey comb grid over which suction is created by an exhaust fan. The rotating screen at the bottom imparts a specific amount of angular momentum to the in-rushing air. The honeycomb grid divorces the far vortex from the flow in the chamber.

---

[2] That cyclonically curved echoes correspond to tornadoes was known from the mid-40's and documented by Stout and Huff (1953). Browning and Ludlam (1962) first correctly identified the weak echo region as updraft; Browning (1965) later explained the hook as a consequence of updraft rotation.

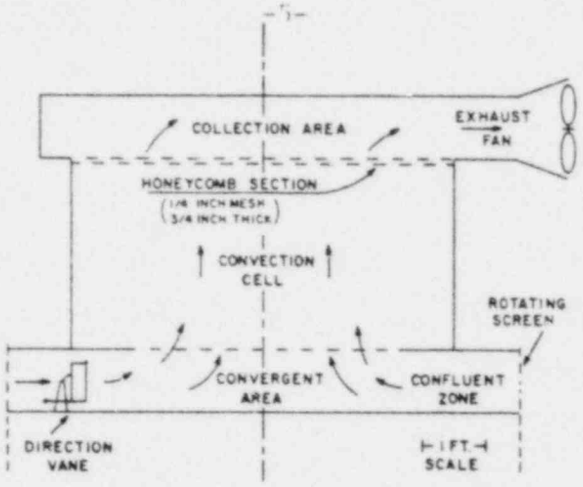

Fig. 1a. Vertical section of laboratory device. (After Ward, 1972.)

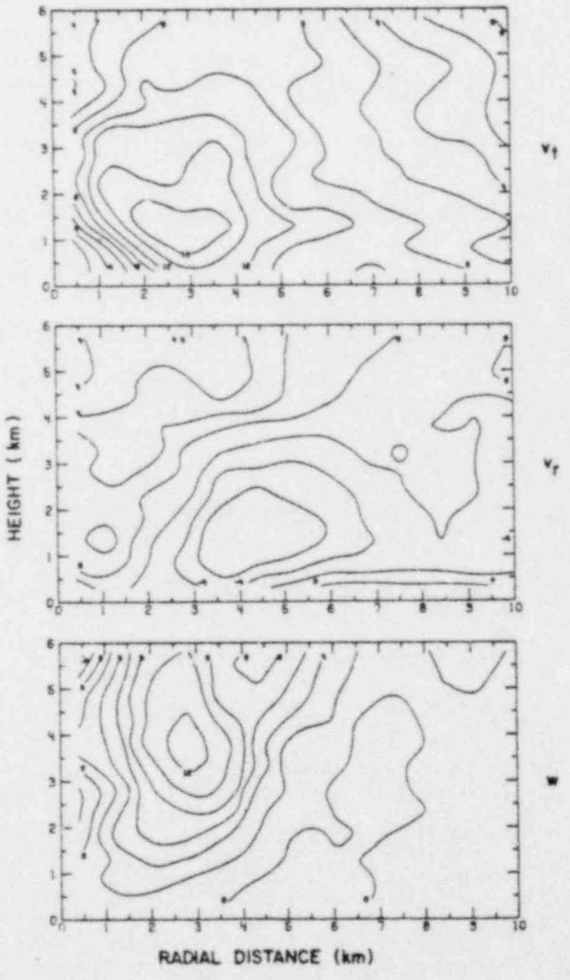

Fig. 1b. Radial-height distributions of mean tangential (v_t), radial (v_r), and vertical (w) wind while tornado is on the ground (1553 CST). Positive velocities (m s^{-1}) designate cyclonic, outward and upward motion. Radial distances are from the mesocirculation vertical axis. (After Brandes, 1978).

The basic physical mechanism is simply that given enough time, low-level convergence beneath a storm updraft can cause air parcels with non-zero angular momentum (radius times tangential velocity) to decrease their radius with respect to the updraft center and, if they conserve their angular momentum, increase their tangential velocity. A recent synopsis (Lemon and Doswell, 1979) of the available observations note that the rotating wind field is colocated with the storm updraft at early stages in a storm's history and at later stages a downdraft develops in the storm's rear flank; the rotation of the wind field then is nearly centered on the boundary between updraft and downdraft with the tornado forming on the updraft side. This observation has lead to speculation as to the role of the thunderstorm downdraft in tornadogenesis. Lemon and Doswell (1979) suggest that since rather sharp temperature and pressure variations occur horizontally across the updraft/downdraft boundary that the vertical component of the baroclinicity vector ($\nabla\rho \times \nabla P$) could enhance the vertical component of vorticity. However, this effect is non-Boussinesq and according to Lemon and Doswell the maximum value of ($\nabla\rho \times \nabla P$) is still smaller than the minimum values of the vortex tilting and stretching terms in the vertical vorticity equation (see their Table 1). We favor the following explanation: The downdraft being cold and heavy tends to spread horizontally upon reaching the ground and, further, originates at a level where the horizontal momentum is different from the momentum (wind speed) near the ground, hence the downdraft acts to produce large convergence. Examination of the equation for the vertical vorticity (see e.g., Rotunno, 1981) indicates that the convergence term leads to exponential growth of the vertical component of the vorticity vector (for $\partial w/\partial z > 0$). Hence, the basic mechanism of updraft convergence acting

in conjunction with a source of rotation is still viable vis-a-vis recent observations which indicate an important role for the storm downdraft. One further point, which is sometimes overlooked is that the axisymmetric vortex model does include the effect of vortex tilting (see, Rotunno, 1980). Hence, theories which give prominent role to tilting of horizontal vortex lines into the vertical one are not excluded from consideration by such models.

3.0 Review of Laboratory Model and Axisymmetric Solutions

Although no internal flow measurements were reported by Ward, a number of physical flow features could be ascertained from flow visualization techniques. Perhaps the most important piece of information obtained by Ward was that the core size of the small-scale vortex could be controlled by certain combinations of power-setting on the exhaust fan and rotation rate of the inflow screen. This combination is quantified by consideration of the swirl ratio, which is proportional to the ratio of the angular momentum supplied to the in-rushing air at the screen ($2\pi\Gamma_R$) to volume rate of flow (divided by the radius) through the chamber $2\pi \frac{Q}{R}$. Thus, the swirl ratio is defined

$$S \equiv \frac{R\Gamma_R}{2Q} \tag{3.1}$$

We've yet to define what we mean by 'core size'. In many studies 'core' denotes the radius at which the maximum azimuthal (or, synomously, tangential) velocity occurs. In the case of the familiar Rankine vortex (see e.g., Lamb, 1932) this is the radius at which the inner part, which exhibits solid body rotation, is separated from an outer irrotational flow. We have in the past differed with this definition. In comparing our results with the flow

visualization experiments, we found (Rotunno, 1977) that the streamline which bounds the flow below separated from the surface at a certain radius and thereafter continues almost vertically out the top of the domain, thus, producing a pattern of flow where all of the swirling, inrushing air is deflected upwards at r_c and thereafter exits through the 'top' of the device. So as not to leave a vacuum in the region within r_c, air flows vertically downward through the top. Thus we may imagine a cylindrical boundary within the fluid where the radial velocity, u is approximately zero. If, now, smoke (or any other tracer) is released within r_c and near the ground the smoke will fill this cylindrical region thus making visible a 'core'. This core size was found by Davies-Jones to depend on S. Rotunno (1977) who identified the radius of the separated boundary streamline with the size of the smoke-filled core of Ward's experiment found very good agreement between the lab-measured core-size as a function of swirl ratio, $r_c(S)$ and that which resulted from the numerical integrations. Fig. 3.1 is an example of the type of solutions obtained.

Note the zero streamline separates at radius r_c; the strong variations in the circulation implies that all three components of vorticity are non-zero within the core zone.

Theoretical analysis of this type of flow are along the following lines: A non-rotating updraft may be thought of as being 'driven' by a pressure drop across the device, i.e., there is a conversion from potential to kinetic energy. Now, if angular momentum is imparted to fluid parcels as they enter, and if that angular momentum is conserved, the tangential velocity will increase with decreasing radius. This velocity cannot increase indefinitely since the kinetic energy will become much larger than the pressure drop available

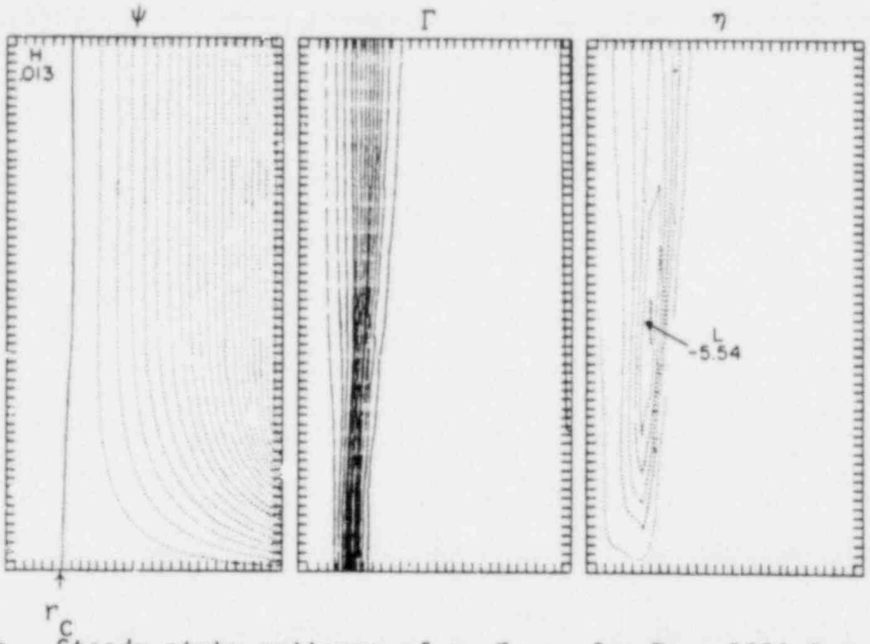

Fig. 3.1a. Steady state patterns of ψ, Γ, η, for Re = 1000 S = .4. In this and all subsequent contour plots, dashed lines signify negative values. The specified inflow velocity is the constant u_0, hence $\psi(R,z)=Ru_0z$ for $0<z<h$. In all experiments u_0 = -1.0 ft s^{-1} and R = 2 ft, thus $\psi(R,z)$ = $-(2.0$ ft $s^{-1})z$ for $0<z<h$ and is $-(2.0$ ft^2 $s^{-1})h$ for $z>h$. Since h=1.0 ft, ψ_{min} = 02.0 ft$^3 s^{-1}$. ψ is contoured in intervals of 0.1 ft$^3 s^{-1}$ starting from the zero value at the axis and lower boundary. (After Rotunno, 1977).

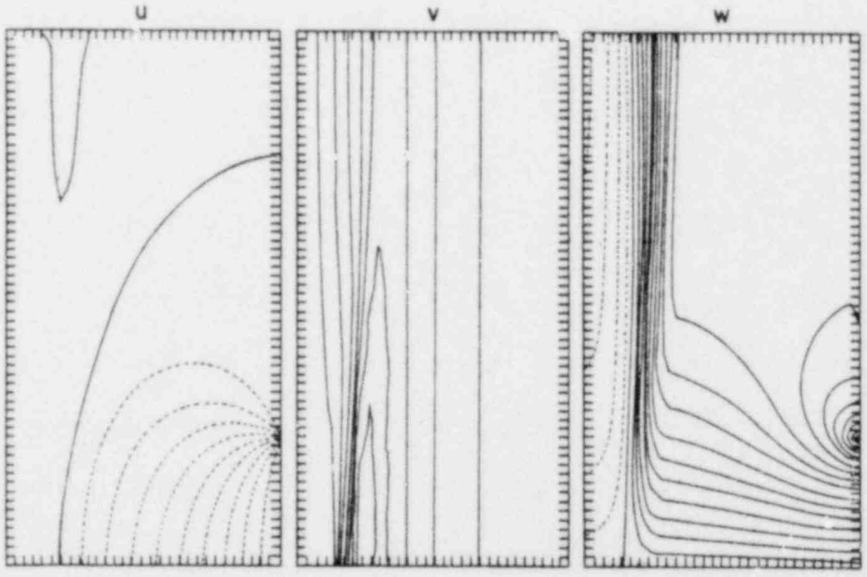

Fig. 3.1b. The steady-state patterns of u, v, and w for Re=1000 and α= 22°. The solid line cutting across the u contour plot is the zero line to the right of which the flow is inward and decelerating from the inlet value of -1.0 ft s^{-1}. The contour interval is 0.1 ft s^{-1}. The v field is contoured every 0.2 ft s^{-1}, starting with the zero axis value v increases outward until the core is reached, then v decreases as r^{-1} to the inlet value of 0.4 ft s^{-1}. The solid line separating the dashed and solid lines in the w contour plot is the zero velocity line. The w field is contoured every 0.1 ft s^{-1}.

to drive the flow. Thus, it is hypothesized that the flow will not reach the center axis and separates at some finite radius r_c. This radius cannot be too large for if $r_c \approx R$, a too large pressure drop would be required to pass a specified volume flow through the thin annular ring. For a full discussion see Lewellen (1971) and Davies-Jones (1973).

The preceding discussion pertains to model solutions employing a free-slip (or zero stress) lower boundary condition. When no-slip conditions are employed the numerical solutions indicate an increased inward penetration of the flow near the bottom boundary (see Fig. 3.2).

There are a number of ways to interpret this; perhaps the most popular is as follows: the flow near and directly influenced by the surface is termed the inner or boundary layer flow. Above the boundary layer and near the core wall the flow is in approximate cyclostrophic balance (radial pressure gradient balances centrifugal acceleration). In the boundary layer the centrifugal acceleration goes to zero, but the pressure gradient remains nearly the same. So, there is an unbalanced inward pressure gradient which produces a radially inward velocity. Once out of the influence of the boundary the flow returns to the situation described above. An interesting feature obtained by Lewellen and Teske (1977) and Rotunno (1979) is that the radially inwards boundary layer flow having angular momentum (albeit weaker than the free-streamvalues) can converge to such a small radius as to produce a higher azimuthal velocity than would be obtained in the free-slip experiments. Both in the laboratory (Church et al., 1979) and in photogrametric analysis (e.g., Golden and Purcell, 1975) the maximum velocities are observed very close to the lower surface.

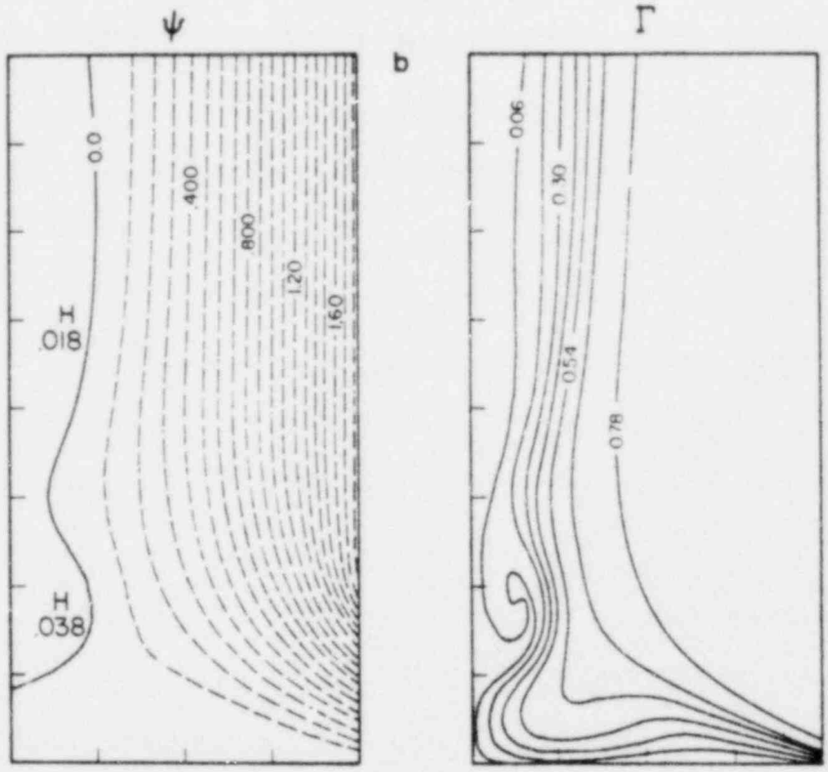

Fig. 3.2. Streamfunction and circulation for S = 0.4, Re = 10^3 at t = 15. (After Rotunno, 1979.)

What we will be concerned with for the major portion of this work is the three-dimensional version of the flow of Fig. 3.1. For small values of S, the vortex is axisymmetric, and so the axisymmetric models are sufficient. However, for larger S, the laboratory vortex becomes highly asymmetric forming multiple vortices. Fig. 3.3 is taken from a flow visualization experiment which shows the highly asymmetric nature of the vortex. As described in the introduction, this frequently occurs in nature. It has been hypothesized by Ward (1972), Davies-Jones and Kessler (1974), Rotunno (1978), and Snow (1978) that these multiple vortices originate as an instability of the basic axisymmetric vortex. In the next section we examine the extant stability theory concerning the type of flow encountered in our model.

4.0 Some Stability Theory

A feature of immense importance in Fig. 3.1 is the sharp radial gradient of Γ and W at $r = r_c$. The flow is obviously stable to <u>axisymmetric</u> disturbances by Rayleigh's (1916) criterion, viz.

$$\frac{d\Gamma^2}{dr} > 0 \tag{4.1}$$

and is (in this case) stable to axisymmetric disturbances by Howard and Gupta's (1962; hereafter referred to as HG) generalization of Rayleigh's criterion, viz.

$$\frac{1}{r^3}\frac{d\Gamma^2}{dr} > \frac{1}{4}\left(\frac{dW}{dr}\right)^2 \quad \text{everywhere for stability (efs)} \tag{4.2}$$

Fig. 3.3. Flow visualization of two multiple vortices in a Ward-type vortex simulator. (After Church et al., 1979.)

(Rayleigh's criterion is recovered with W = constant). However, it is possible (and, in fact likely as we shall demonstrate) that the flow shown in Fig. 3.1 is unstable to asymmetric disturbances. General results, analogous to (4.1) or (4.2) for three-dimensional disturbances for arbitrary (Γ) and W(r) are lacking (see, HG). HG derive the criterion

$$\frac{k^2}{r^3}\frac{d\Gamma^2}{dr} - \frac{2km}{r^3}\Gamma\frac{dW}{dr} - \frac{1}{4}\left\{\frac{kdW}{dr} + m\frac{d}{dr}\frac{\Gamma}{r^2}\right\}^2 \geq 0 \text{ efs} \qquad (4.3)$$

where (m,k) are the azimuthal and vertical wavenumbers, respectively. For m = 0, the axisymmetric criterion is recovered. However, for $m \neq 0$, HG note that as $k \to 0$, criterion (4.3) can <u>never</u> be satisfied. This does not imply instability, only that one cannot be certain the flow is stable. To appreciate this, consider the stability of the Rankine vortex to a three dimensional disturbance (Lord Kelvin, 1880). The Rankine vortex has W = 0 and

$$\Gamma = \omega r^2 \qquad r \leq a$$
$$= \omega a^2 \qquad r \geq a$$

So, criterion (4.3) is that

$$4k^2a^2 \geq 0 \qquad r \leq a$$
$$-m^2\frac{\omega^2 a^4}{r^6} \leq 0 \qquad r > a$$

Clearly, we cannot be assured that the flow is stable. However, Kelvin's analysis proves that the Rankine vortex is stable to three-dimensional disturbances. HG also derive a relation analogous to that used in the

derivation of Rayleigh's theorem on the necessity of an inflection point for instability of parallel inviscid flow (Rayleigh, 1880). Rayleigh's result is that a swirling flow with mean vorticity a monotonic function of r is stable to two-dimensional perturbations. The flow shown in Fig. 3.1 is one where the swirling flow is approximately ze o within an inner core, thus the vorticity is zero. The adjoining annular region where Γ sharply increases with radius is one of high vorticity. Finally, the flow for larger radius has Γ = const., i.e., there is zero vorticity. Hence Rayleigh's necessary condition for instability to two-dimensional disturbances is satisfied.

Consider now the stability of non-swirling ($\Gamma = 0$) axial flow W(r). Again, criterion (4.3) is not of much use. Rayleigh (1892) found that a sufficient condition for stability is that

$$\frac{d}{dr}\left(\frac{r}{m^2+k^2r^2}\frac{dW}{dr}\right) \quad \text{Not change sign for any r (ncs)}$$

For axisymmetric perturbations (m=0), the criterion is that for stability

$$\frac{d}{dr}\left[\frac{1}{r}\frac{dW}{dr}\right] \qquad \text{(ncs)} \tag{4.4}$$

For two-dimensional perturbations (k=0), the criterion is that for stability

$$\frac{d}{dr}\left[r\frac{dW}{dr}\right] \qquad \text{(ncs)} \tag{4.5}$$

This point merits some discussion. Bergman (1969) notes that this relation is irrelevant since by setting k=0, the perturbation equations are 'unaware' of W and therefore the disturbances are stable in this limit. This contrasts

with the statement made by Batchelor and Gill (1962) for the 'top-hat'profile, viz. "The flow is unstable to a small disturbance for all values of n(or m) and a(or k)." For $m,k \to 0$, Batchelor and Gill (1962) find that c_i (the imaginary phase speed) is zero, thus the flow is stable to this trivial disturbance. For $m \neq 0$, $k \to 0$ they find that $c_i \to$ constant; this is true, however the actual growth rate ($=kc_i$) tends to zero. Hence purely two-dimensional disturbances are stable.

The criteria cited above are the only general criteria extant and are in fact too weak to be of great utility. Hence, the approach has been to examine the stability characteristics of special profiles $\Gamma(r)$, $W(r)$ as the need to know those characteristics arose. For an exhaustive review of work in this area the reader is advised to see Bergman (1969). Also in that work is a stability analysis of some "two-celled' vortex solutions (Sullivan, 1959; Kuo, 1967) similar to those of Fig. 3.1 We shall not repeat such calculations because this amounts to a numerical solution of the linearized equations of motion which is somewhat superfluous since we are computing the solution to the full non-linear, viscous equations of motion. However, we shall always check that the axisymmetric flow may be unstable according to the above criteria. Further, in view of the above-cited analytical problems, we must proceed on somewhat heuristic arguments. One heuristic argument which we shall appeal to is that the radial shear of W is primarily responsible for the instability of axisymmetric ($m \neq 0$, $k=0$) disturbances (as long as $\partial\Gamma^2/\partial r > 0$) while the radial shear of V is responsible for the instability of angular disturbances ($m \neq 0$, $k=0$); flows with non-zero V and W might have a most unstable mode (m,k) where m is determined mainly by V(r) and k by W(r). We shall return to this discussion in the chapter "Interpretations".

5.0 The Numerical Model

The model developed here follows that of Williams (1969) closely. Williams developed a numerical model to study the flow in a rotating, differentially heated annulus; the Boussinesq equations are solved in cylindrical coordinates. Hence, much of Williams' work can be carried over directly. So, unless otherwise stated the model description in this section is identical, to William's. Our system is simpler, in one respect, because we have no thermal effects and need not solve a temperature equation, however, in another respect it is more problematic (i.e., fluid may pass into or out of the domain).

5.1 Governing Equations

The governing equations for a constant density, constant viscosity fluid in cylindrical coordinates (r, θ, z) are

$$\frac{Du}{Dt} - \frac{v^2}{r} = - P_r + Re^{-1} F(u) \tag{5.1}$$

$$\frac{Dv}{Dt} + \frac{uv}{r} = - \frac{P_\theta}{r} + Re^{-1} I(v) \tag{5.2}$$

$$\frac{Dw}{Dt} = - P_z + Re^{-1} H(w) \tag{5.3}$$

$$\frac{1}{r} (ru)_r + \frac{1}{r} v_\theta + w_z = 0$$

where

$$(u,v,w) = \frac{1}{u_R} (u',v',w'); \qquad P = \frac{P'}{u_R^2}; \qquad (z,r) = \frac{1}{R} (z',r')$$

where u', v', w', are the dimensional components of the velocity vector in the r', θ, z' directions, respectively; P' is the dimensional pressure divided by density and Re is the Reynolds number $u_R R/\nu$ based on the inflow speed u_R, chamber radius R and eddy viscosity ν. Subscripts denote partial differentiation.

$$\frac{D}{Dt} q \equiv \frac{\partial q}{\partial t} + \frac{1}{r} \frac{\partial}{\partial r} (ruq) + \frac{1}{r} \frac{\partial}{\partial \theta} vq + \frac{\partial}{\partial z} wq \tag{5.5}$$

Also,

$$F(u) = u_{zz} + \frac{1}{r^2} u_{\theta\theta} - w_{rz} - \frac{1}{r^2} (rv_\theta)_r \tag{5.6}$$

$$I(v) = \left(\frac{1}{r} (rv)_r\right)_r + v_{zz} - \left(\frac{u_\theta}{r}\right)_r - w_{\theta z} \tag{5.7}$$

$$H(w) = \frac{1}{r} (rw_r)_r + \frac{1}{r^2} w_{\theta\theta} - \frac{1}{r} v_{r\theta} - \frac{1}{r} (ru_z)_r \tag{5.8}$$

In vector notation the system of equations (5.1) is

$$\frac{\partial \mathbb{V}}{\partial t} + \mathbb{V} \cdot \nabla \mathbb{V} = - \nabla P - Re^{-1} \nabla \times \omega \tag{5.9}$$

$$\nabla \cdot \mathbb{V} = 0 \tag{5.10}$$

where $\omega = \nabla \times \mathbb{V}$ is the vorticity vector. Equation (5.9) is prognostic for $\mathbb{V}$; to obtain P given $\mathbb{V}$, we take $\nabla \cdot$ (5.9) using (5.10) to obtain

$$\nabla^2 P = - \nabla \cdot \{\mathbb{V} \cdot \nabla \mathbb{V}\}$$

which is an elliptic equation for P. The boundary conditions on P are obtained from (5.9) and are discussed below.

5.2 Governing Equations in Discrete Form, Domain and Grid System

The domain is a right circular cylinder which covers the central part of the vortex chamber shown in Fig. (5.1). Fluid enters through the sidewall for $0 \leq z \leq h/R$ (=.5) and may leave or enter through the top ($z = H/R = 2$) for $a \leq r \leq 1$. A small center annulus (which does not exist in the laboratory or nature) is put into our model so as to avoid the severe time-step limitations imposed by the very small ($O(r\Delta\theta)$) azimuthal grid lengths. We will argue below that for the cases under present study the existence of the annulus does not seriously alter the main conclusions. The model domain is as depicted in Fig. 5.1. Boundary conditions are also indicated and will be explained subsequently.

Fig. 5.2 contains the grid system. The coordinates of the P points $P_{i,j,k}$ are at

$$r_i = (i-.5)\Delta r + a \qquad i = 1,M$$

$$\theta_k = (k-1)\Delta\theta \qquad k = 1,L$$

$$z_j = (j-.5)\Delta z \qquad j = 1,N$$

where

$$\Delta r = \frac{1-a}{M}, \qquad \Delta\theta = \frac{2\pi}{L}, \qquad \Delta Z = \frac{2}{N}$$

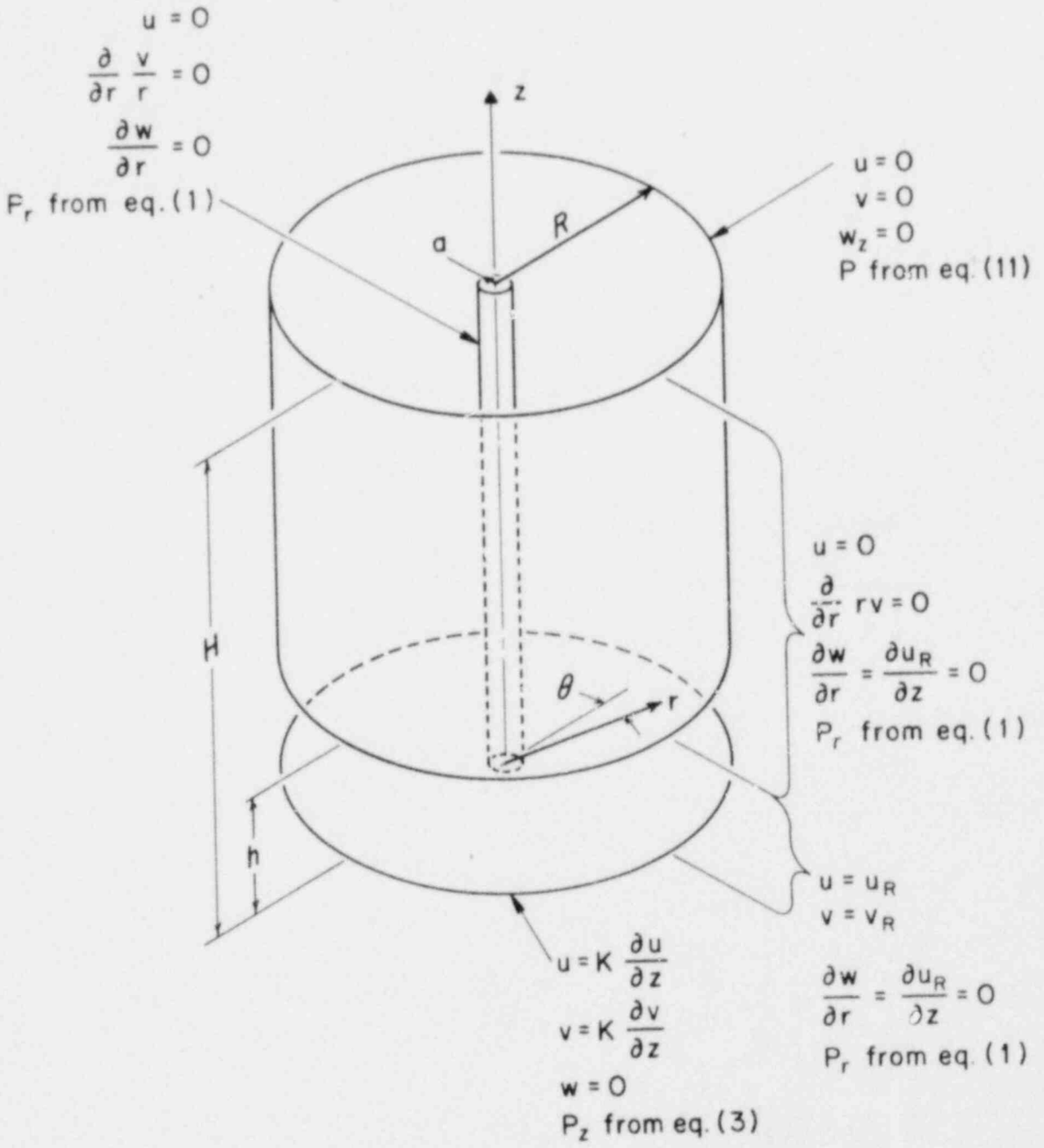

Fig. 5.1. Schematic of computational domain, boundary conditions are indicated.

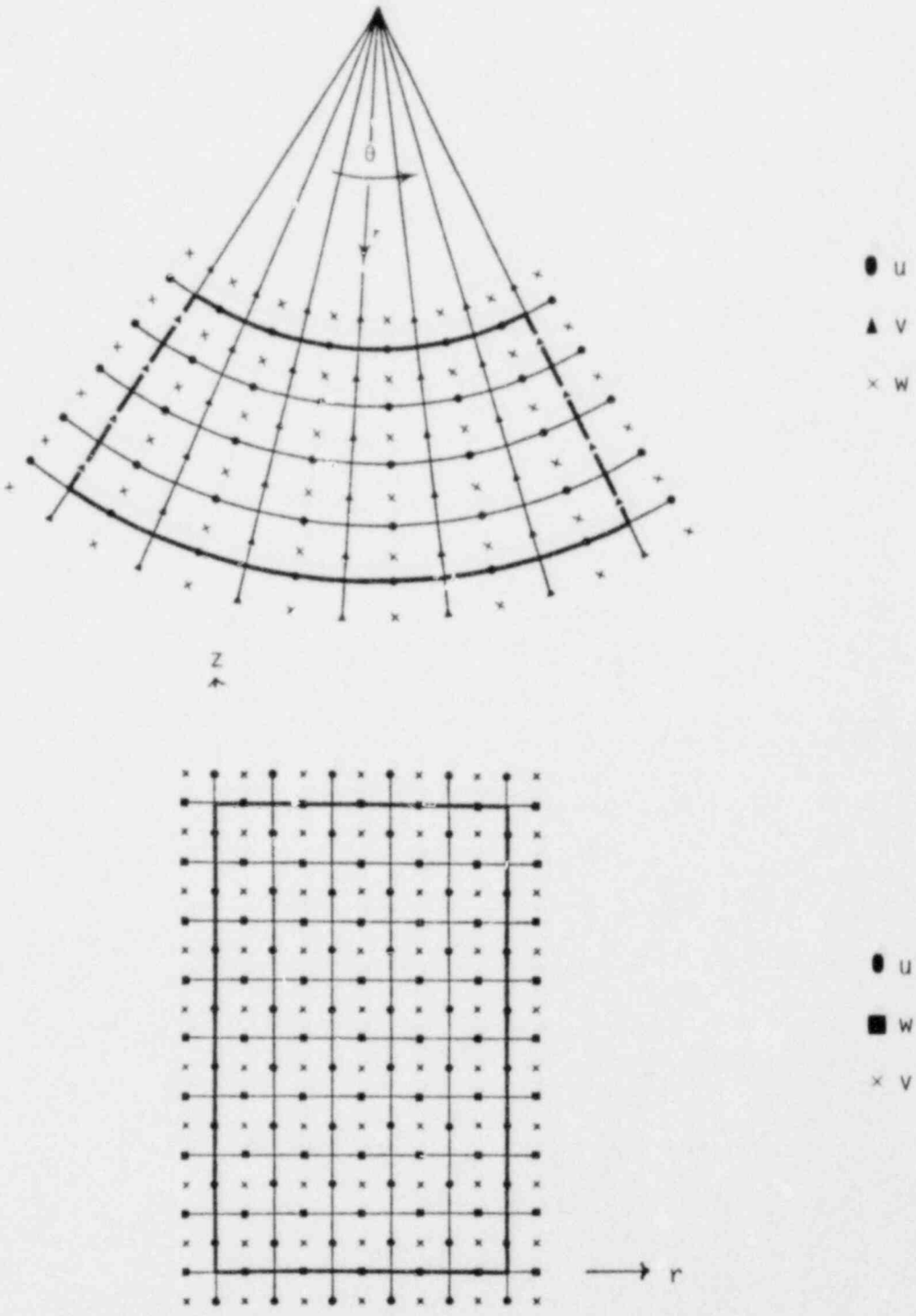

Fig. 5.2. Schematic of grid arrangement. (After Williams, 1969)

where M, L, N are number of gridpoints in the r, θ, and z directions, respectively. For this study we use M=30, L=32, and N=30.

The other variables are defined similarly

$$u_{i,j,k} \quad \begin{cases} r_i = (i-1)\Delta r + a & i = 1,M+1 \\ \theta_k = (k-1)\Delta\theta & k = 1,L \\ z_j = (j-1.5)\Delta z & j = 1,N+2 \end{cases}$$

$$v_{i,j,k} \quad \begin{cases} r_i = (i-1.5)\Delta r + a & i = 1,M+2 \\ \theta_k = (k-.5)\Delta\theta & k = 1,L \\ z_j = (j-1.5)\Delta z & j = 1,N+2 \end{cases}$$

$$w_{i,j,k} \quad \begin{cases} r_i = (i-1.5)\Delta r + a & i = 1,M+2 \\ \theta_k = (k-1)\Delta\theta & k = 1,L \\ z_j = (j-1)\Delta z & j = 1,N+1 \end{cases}$$

The time variable t is discretized by setting $t = \tau\Delta t$ where Δt is the time-step. With the shorthand notation

$$\delta_x q = [q(x + \tfrac{1}{2}\Delta x) - q(x - \tfrac{1}{2}\Delta x)]/\Delta x$$

$$\overline{q}^x = [q(x + \tfrac{1}{2}\Delta x) + q(x - \tfrac{1}{2}\Delta x)]/2$$

the governing equations are written

$$\delta_t \overline{u}^t + \frac{1}{r}\delta_r(\overline{ru}^r\overline{u}^r) + \frac{1}{r}\delta_\theta(\overline{v}^r\overline{u}^\theta) + \delta_z(\overline{w}^r\overline{u}^z) - \frac{\overline{v^2}^{r\theta}}{r} \tag{5.12}$$

$$= -\delta_r P + \nu F^*(u)$$

$$\delta_t \overline{v}^t + \frac{1}{r}\delta_r(\overline{ru}^\theta\overline{v}^r) + \frac{1}{r}\delta_\theta(\overline{v}^\theta\overline{v}^\theta) + \delta_z(\overline{w}^\theta\overline{v}^z) + u\frac{\overline{rv}^{r\theta}}{r^2} \tag{5.13}$$

$$= -\delta_\theta P + \nu I^*(v)$$

$$\delta_t \overline{w}^t + \frac{1}{r}\delta_r(\overline{ru}^z\overline{w}^r) + \frac{1}{r}\delta_\theta(\overline{v}^z\overline{w}^\theta) + \delta_z(\overline{w}^z\overline{w}^z) \tag{5.14}$$

$$= -\delta_z P + \nu H^*(w)$$

$$\frac{1}{r}\delta_r(ru) + \frac{1}{r}\delta_\theta v + \delta_z w = 0 \tag{5.15}$$

where

$$F^*(u) \equiv \left[\delta_{zz}u + \frac{1}{r^2}\delta_{\theta\theta}u - \delta_{rz}w - \frac{1}{r^2}\delta_r(r\delta_\theta v)\right]_{lag} \tag{5.16}$$

$$I^*(V) \equiv \left[\delta_r\left(\frac{1}{r}\delta_r(rv)\right) + \delta_{zz}v - \delta_{r\theta}\left(\frac{u}{r}\right) - \frac{1}{r}\delta_{z\theta}w\right]_{lag} \tag{5.17}$$

$$H^*(w) \equiv \left[\frac{1}{r}\delta_r(r\delta_r w) + \frac{1}{r^2}\delta_{\theta\theta}w - \frac{1}{r}\delta_{z\theta}v - \frac{1}{r}\delta_{rz}(ru)\right]_{lag} \tag{5.18}$$

Instead of rewording Williams' description of this system, we take the liberty of direct quotation:

"The expressions and operator notation must be interpreted with respect to the grid-point of the variable under consideration. The centered time differencing is for the level τ so that the predictions yield the variables at level $(\tau + 1)$. The non-linear rotational and pressure terms are evaluated at the central level τ whereas the diffusive terms use the non-central $(\tau - 1)$ level, denoted by the subscript 'lag'. The continuity equation (5.15) applies at a point and is valid for the fluid unit surrounding that point. The averaging in the equations is necessary to provide variables values at grid points where the variables are not explicitly defined. Through using an interlacing grid system the amount of averaging of this type is reduced to a minimum thus improving accuracy. Furthermore, the continuity equation has a unique exact form which can only be achieved by such a grid; this uniqueness is essential for deriving the Poisson equation. The only disadvantage occurs in the rotational terms, where products such as uv must be averaged as u and v occur at different locations."

The following is also nearly a quotation of Williams.

The variables u, v, and w may be obtained by marching equations (5.12)-(5.14). To obtain P and satisfy continuity, a Poisson equation must be derived. To achieve this, suppose for convenience that the prediction equations can be written as

$$\begin{aligned} \delta_t \bar{u}^t &= -\delta_r P + GU \\ \delta_t \bar{v}^t &= -\frac{1}{r}\delta_\theta P + GV \\ \delta_t \bar{w}^t &= -\delta_z P + GW \end{aligned} \tag{5.19}$$

where $\underset{\sim}{G} = (GV, GU, GW)$ represents the non-linear, viscous and rotational terms. Substituting these equations into the continuity equation (5.15) gives

$$\nabla^2 P = \nabla \cdot \underset{\sim}{G} \tag{5.20}$$

where

$$\nabla^2 P \equiv \frac{1}{r}\,\delta_r(r\delta_r P) + \frac{1}{r^2}\,\delta_{\theta\theta} P + \delta_{zz} P$$

and

$$\nabla \cdot \underset{\sim}{G} = \frac{1}{r}\,\delta_r(r\,GU) + \frac{1}{r}\,\delta_\theta GV + \delta_z GW \tag{5.21}$$

Solving (5.20) during each time-step provides the values of P needed to complete the marching process.

In executing the calculation the components of G, can be evaluated from the variables of the previous time step. Forming the divergence of G, the Poisson equation (5.20) on solution gives values of P. Using these values of G and P, the variables u, v, and w at the next time step can then be directly evaluated.

The time step is chosen so as to satisfy the CFL condition and the diffusive stability criteria, viz.

$$\Delta t < \min\left(\frac{r\,\Delta\theta}{v_{max}}\,,\ \frac{\Delta z}{w_{max}},\ \frac{\Delta r}{u_{max}}\right) \tag{5.22}$$

$$\Delta t < \min \frac{Re}{8}\left(r^2\Delta\theta^2,\ \Delta z^2,\ \Delta r^2\right) \tag{5.23}$$

In this study, $\Delta t = .01$ and integrations carried out every several thousand time steps.

5.3 Boundary Conditions

The preceding section describes how u, v, and w are predicted within the domain. Now we describe the condition of the fluid at the boundary of the domain. At r = 1, fluid enters the domain for $0 \leq z \leq .5$ with velocity u = 1 and with a specified azimuthal component $v = v_R$. Since $\Gamma_R = v_R R$ and $Q = u_R Rh$, then from Eq. (3.1)

$$S = \frac{R}{2h} \frac{v_R}{u_R}$$

For this study h/R = .5. Thus v_R/u_R is synonomous with the swirl ratio. For $.5 \leq z \leq 2$, u = 0 at a fictitious wall. At this wall, we require the vertical vorticity to be zero, i.e., $(rv)_r = 0$. Along the entire boundary ($0 \leq z \leq 2$) we require the azimuthal component of the vorticity vector $\eta = u_z - w_r = 0$. Thus $w_r = u_z$, which is prescribed because u is. Since u is prescribed as a time independent function of z at r = 1, we can use equation (5.1) to obtain

$$P_r\Big|_{r=1} = -\frac{D}{Dt} u + \frac{v^2}{r} + Re^{-1} F(u)$$

At r=a, we set u=0 on the impermeable inner annulus, require zero stress ($(v/r)_r = 0$ and $w_r = 0$) and P_r is known at time τ from Eq. (5.1). At the lower boundary we require w = 0 at the impermeable surface and set $(u,v) = K(u,v)_z$, where K is a constant (in dimensional form, K has dimensions of length). When K = 0 the condition u = v = 0 (no-slip), while when $K \to \infty$

the condition becomes $u_z = v_z = 0$ (free-slip). G. I. Taylor (1965) first used this condition for a Ekman layer flow; later Kuo (1971) also employed this condition. P_z is known at from Eq. (5.3). At the upper boundary, $z = 2$, we require the flow exit without radial or tangential velocity; $u = v = 0$. (As is done in the laboratory with a honey comb grid.) This is somewhat different than the conditions used by Rotunno (1977, 1979). In those studies $u = \partial v/\partial z = \partial \eta/\partial z = 0$ (η is azimuthal component of the vorticity vector). The reason for this is as follows. The axisymmetric flow could not have azimuthally travelling waves whereas the present three-dimensional calculation can and does; we found that, in addition to being more faithful to the laboratory apparatus, the present boundary conditions vastly simplify the 'open' boundary condition problem. With $u = v = 0$. Equation (5.1) gives for P_r

$$P_r \Big|_{z=2}^{t=\tau} = -(wu_z)^{\tau} + \nu u_{zz}{}^{\tau-1} \tag{5.24}$$

since the absolute value of P is irrelevant we choose $P(r=a) = 0$ and integrate (5.24) to obtain

$$P(r, \theta, z=2, t=\tau) = \int_a^r \{(-wu_z)^{\tau} + (\nu u_{zz})^{-1}\} dr' \tag{5.25}$$

So, we have pressure at the upper boundary.

5.4 The Poisson Equation (5.20)

This equation is solved exactly as described in Swarztrauber and Sweet (1975), p. 52-56. We describe it here briefly.

Taking advantage of the periodic nature of the problem in the azimuthal direction, the equation (5.20) and the boundary conditions on it are decomposed (using fast Fourier transforms) into L discrete Fourier components, Eq. (5.20) then is reduced to the solution of L two-dimensional elliptic equations (in the r-z plane). The algorithms used to solve the two dimensional solutions are also described in the report cited. With the solutions for the Fourier components in hand, we synthesize them via an inverse FFT to obtain the pressure. The FFT algorithms are part of the standard NCAR software library. A complete copy of the code will be sent to the NRC.

6.0 Results

We shall discuss one particular example (S = 1, Re = 150, free-slip lower boundary condition) in detail. For this particular set of parameters, the numerical solutions exhibit two intertwining helical vortices. Other combinations of the parameters (S, Re) lead to solutions exhibiting more or less multiple vortices, however, the basic physical structure of each individual vortex does not vary as a function of the number of vortices present. Hence, we shall concentrate on an example where only two multiple vortices form and analyze in some detail the associated three-dimensional flow pattern.

Initially, the flow has zero vorticity and v is set to zero everywhere. To obtain the initial u, w fields, we solve the following elliptic equation for u[3] under the boundary conditions discussed in Section 5.3.

---

[3] Obtained by combining the zero vorticity condition

$$u_z - w_r = 0$$

with the continuity equation

$$\frac{(ru)_r}{r} + w_z = 0$$

$$\left(\frac{(ru)_r}{r}\right)_r + u_{zz} = 0 \qquad (6.1)$$

This procedure produces the flow patterns displayed in Fig. 6.1. The flow is initially axisymmetric, and so the r-z cross section in Fig. 6.1 is identical for each of the L(=32) such sections in the domain

Rotation is added for $t > 0$ at $r = 1$ by letting

$$v(r,\theta,z,t) = v_R(1 - e^{-t/t_s}) \qquad 0 \leq z \leq .5$$

which is analogous to slowly (over a time period $t_s = 2$, in all cases) spinning up the rotating screen at the rim of the cylinder of the laboratory model. The swirling flow is then transported inward and upward by the initial u,w field. As explained in Rotunno (1977) and in Section 2, the swirling flow cannot reach a too small radius. Hence, the flow in the r-z plane develops a 'two-celled' structure. By the time $t = 10$, the flow reaches an axisymmetric steady-state configuration similar[4] to that described by Rotunno (1977). Since the initial conditions are axisymmetric to within round-off error, the flow will remain axisymmetric unless it is unstable in which case small asymmetries could grow at an exponential rate. However, even at an exponential growth rate, it may take a long time for the instabilities to develop. Hence to conserve computer time, we add a small amount of random noise at a stage ($t = 6$) of flow development.

---

[4] except for the maximum observed in v near the top; this is due to the condition $v = 0$ and will be discussed in the section entitled 'Interpretations'.

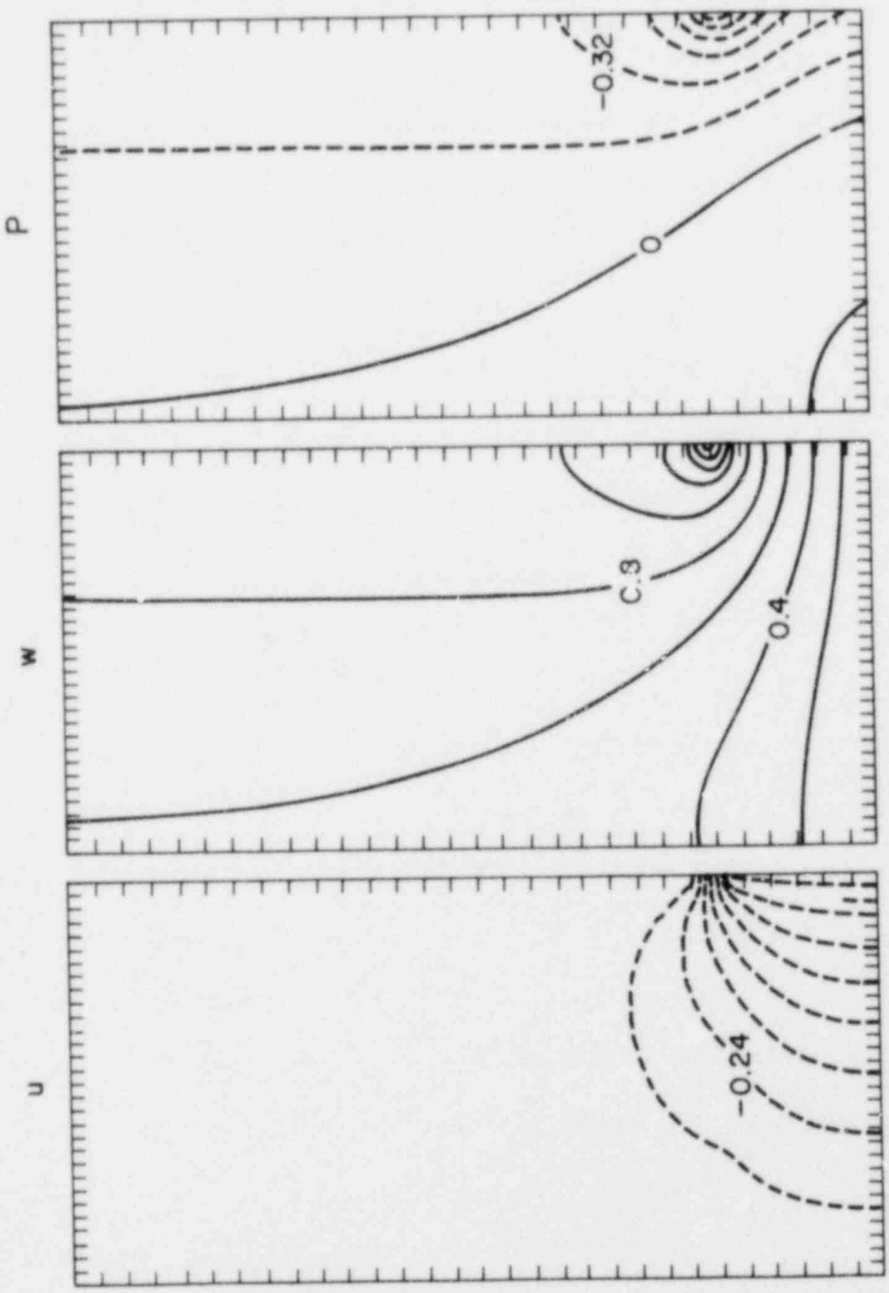

Fig. 6.1. Initial fields of u(r,z), w(r,z), P(r,z) (v(r,z) = 0). Countour values are marked on figure.

The first evidence of flow asymmetry in the horizontal contour plots is at approximately t = 22. Fig. 6.2 a-d contain the azimuthally averaged u, v, w, P fields at t = 20. The flow is still essentially axisymmetric at this time; Fig. 6.3 a-d display horizontal contour plots of u, v, w, P at z = Δz.

Figure 6.3 a-d are included at this point for future reference; the r-contour plots will change drastically as the wave grows to finite amplitude.

Figure 6.4 a-d displays the same cross sections as shown in Fig.s 6.2 a-d at t = 60. The horizontal cross sections at z = Δz are displayed in Fig. 6.5 a-d. Considering the radial velocity together with the tangential velocity, clearly indicates smaller scale rotating wind field within a larger-scale rotating wind field. We identify this smaller scale vortex as the multiple vortex phenomenon. Figure 6.6 is a composite of u, v, w, and P for one of the multiple vortices. Notice the horizontal circulation center nearly coincides with the pressure minimum and lies somewhere near the maximum gradient of w but in the updraft. Just above this low level the pattern is essentially unchanged but shifts clockwise; Fig. 6.7 contains the horizontal contour plot of P which illustrates this behavior. The distance of the MV center from the central axis increases with height and the circulation pattern becomes more diffuse.

The basic pattern shifts counterclockwise in time at a rate

$$\frac{\Delta\theta_{\text{pattern}}}{\Delta t} \sim 1.8$$

which is approximately one half the maximum mean rotation rate of the fluid $(\bar{v}/r)_{max}$ (which occurs at r = 10Δr + a, z = 2Δz).

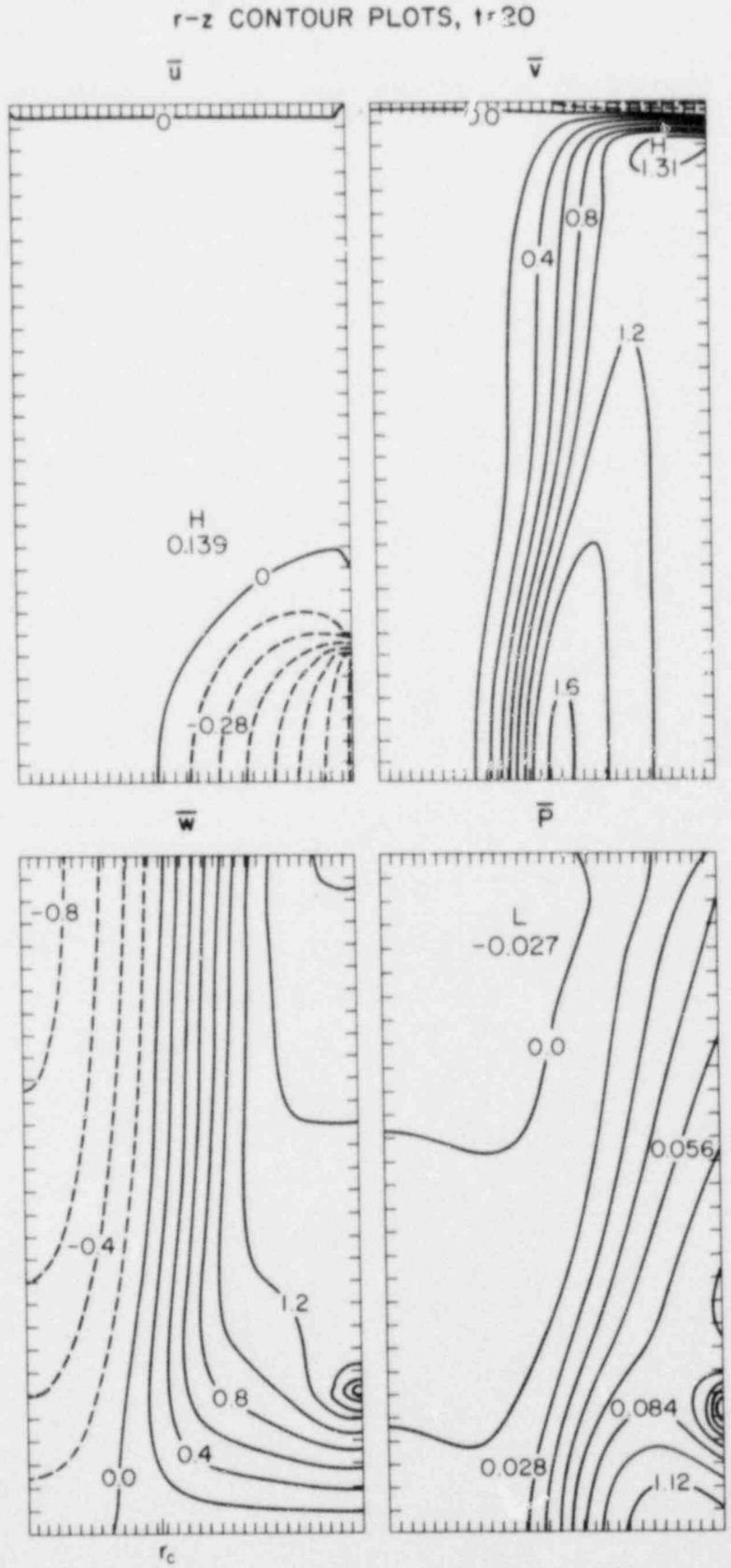

Fig. 6.2. Azimuthally averaged u, v, w, P fields at t = 20. The flow is still essentially axisymmetric at this time.

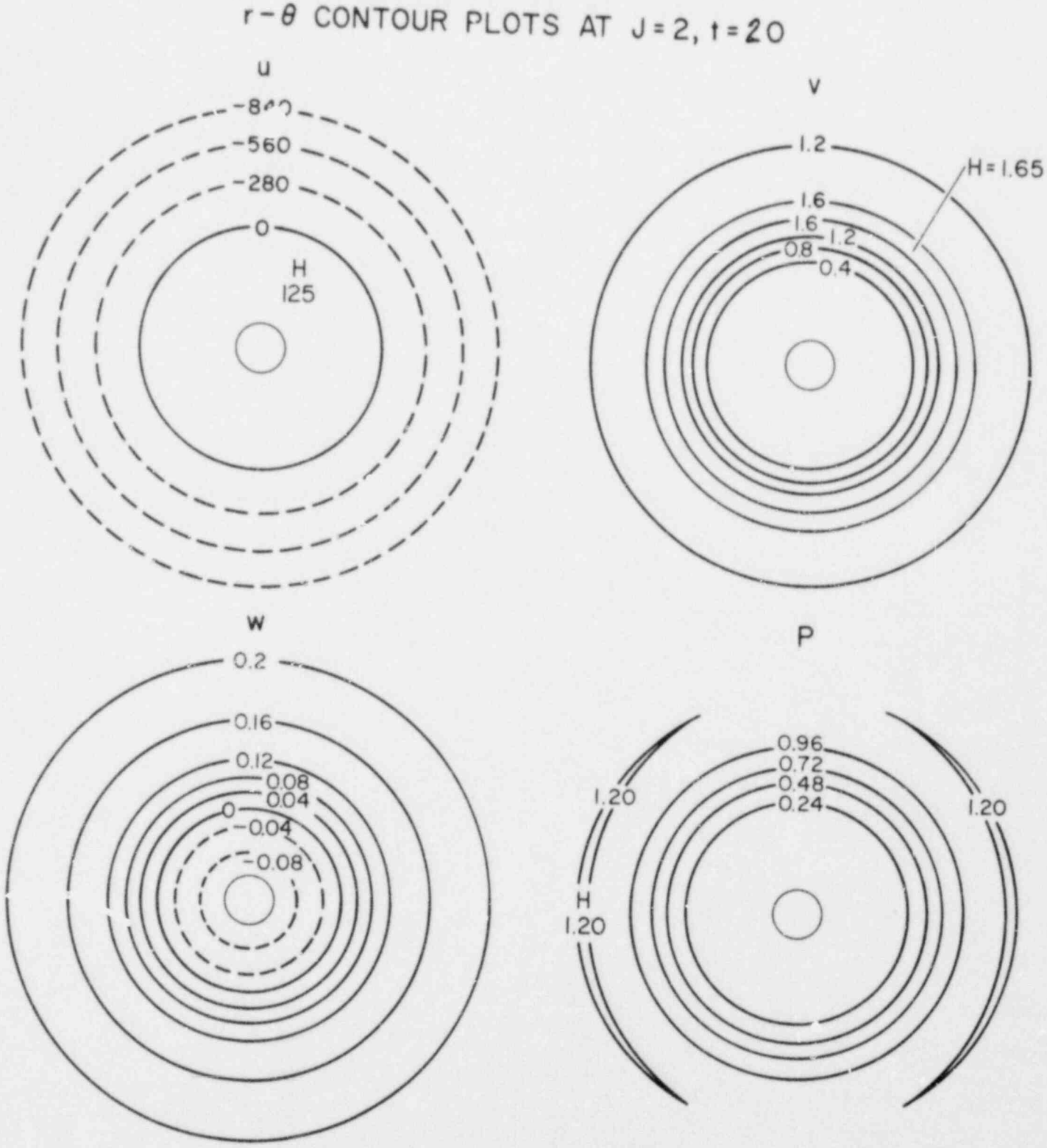

Fig. 6.3 a-d. rθ contour plots of u, v, w, P at z = 2Δz.

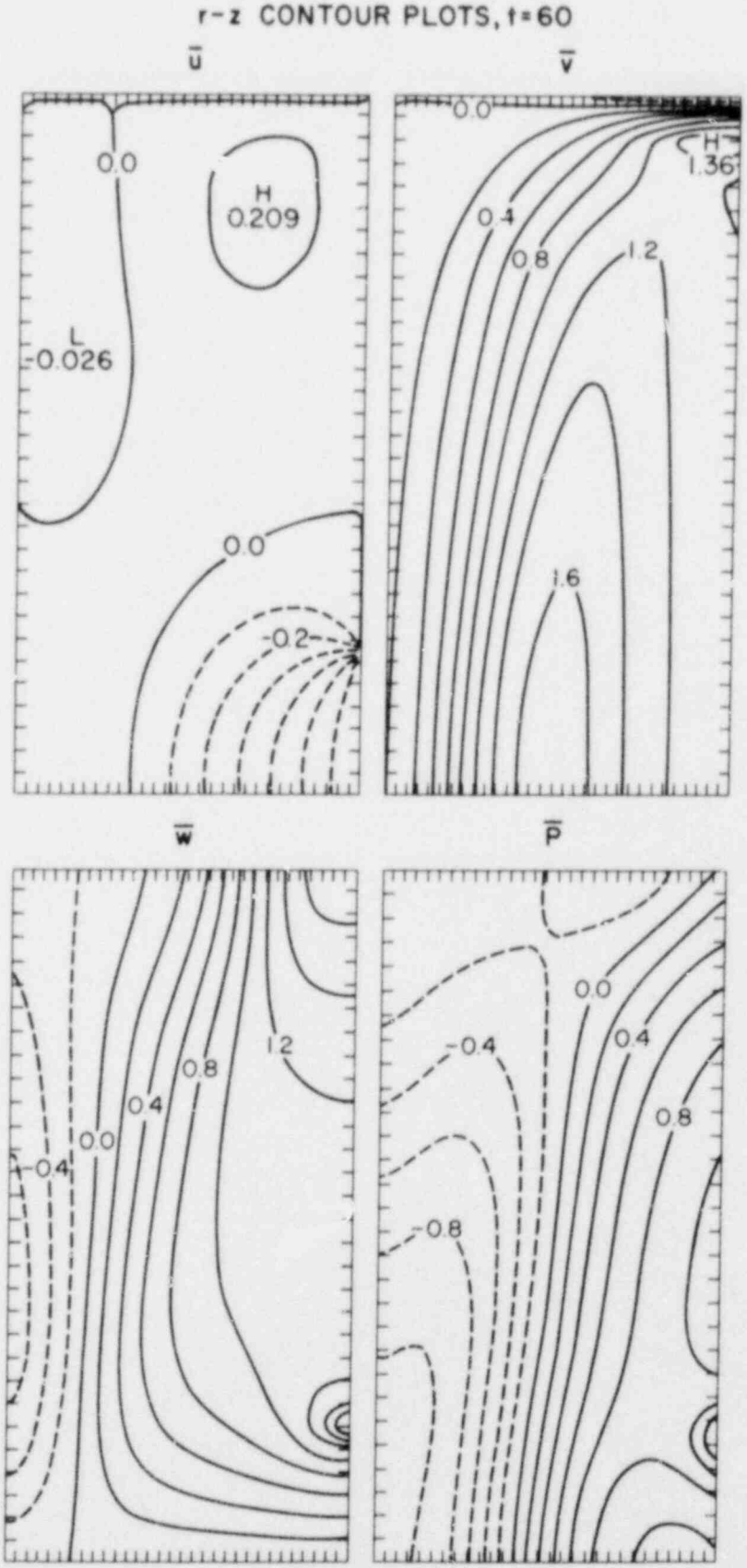

Fig. 6.4 a-d. Same as Fig. 6.2 a-d except t = 60.

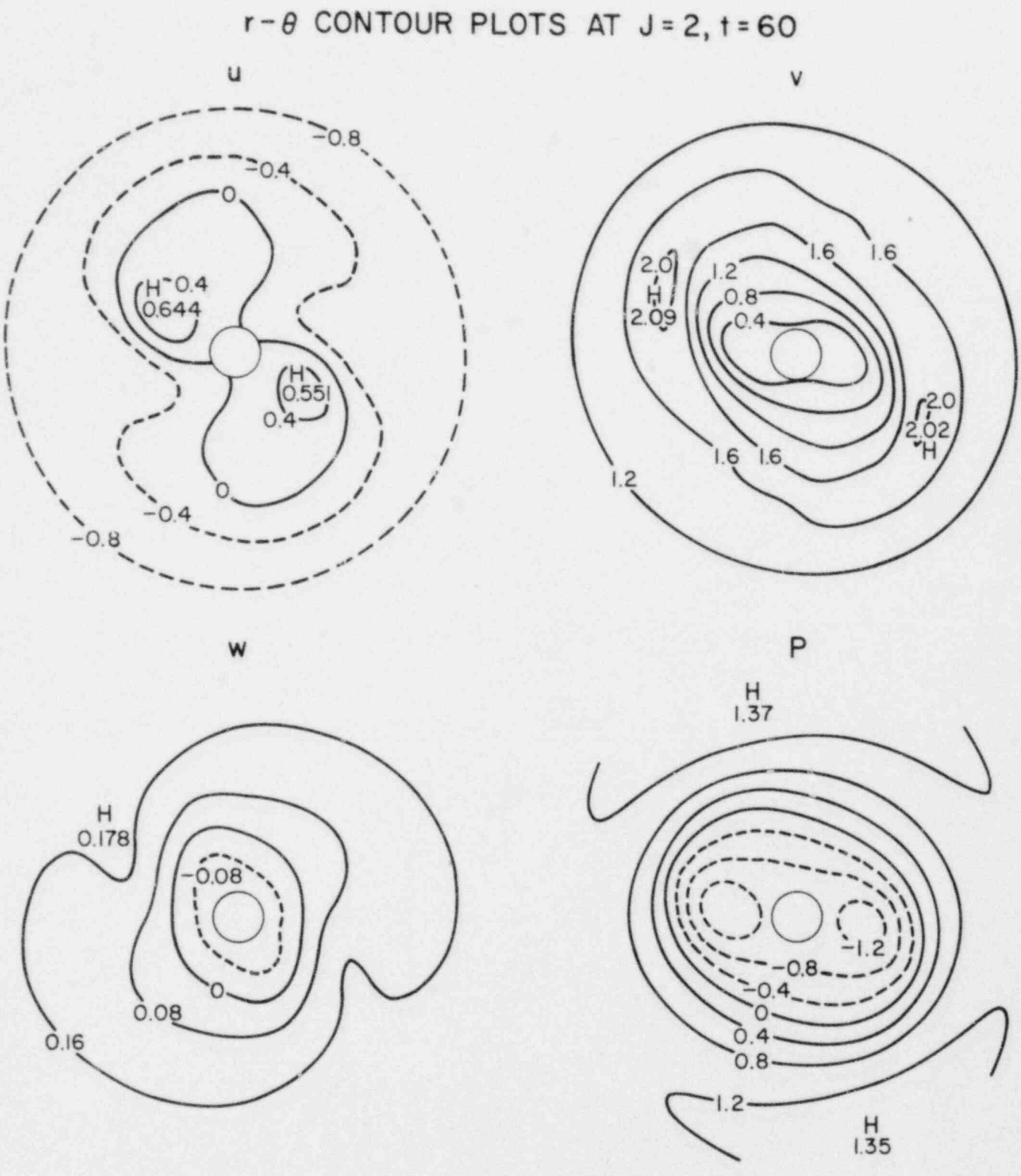

Fig. 6.5 a-d. Horizontal cross sections at z = z of u, v, w, P. Note the smaller scale rotating wind field within the larger scale rotating wind field.

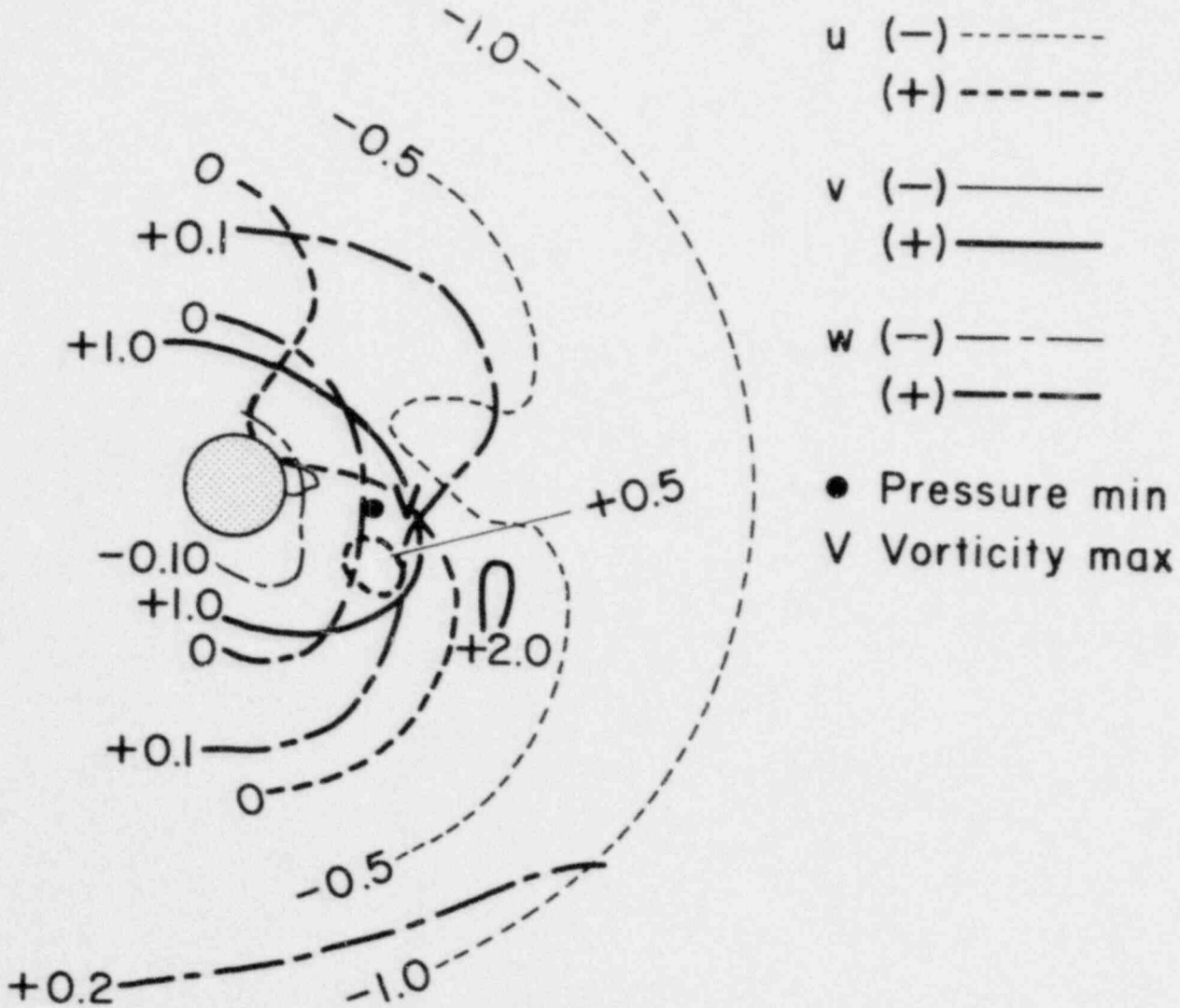

Fig. 6.6. A composite of u, v, w, and P for one of the multiple vortices.

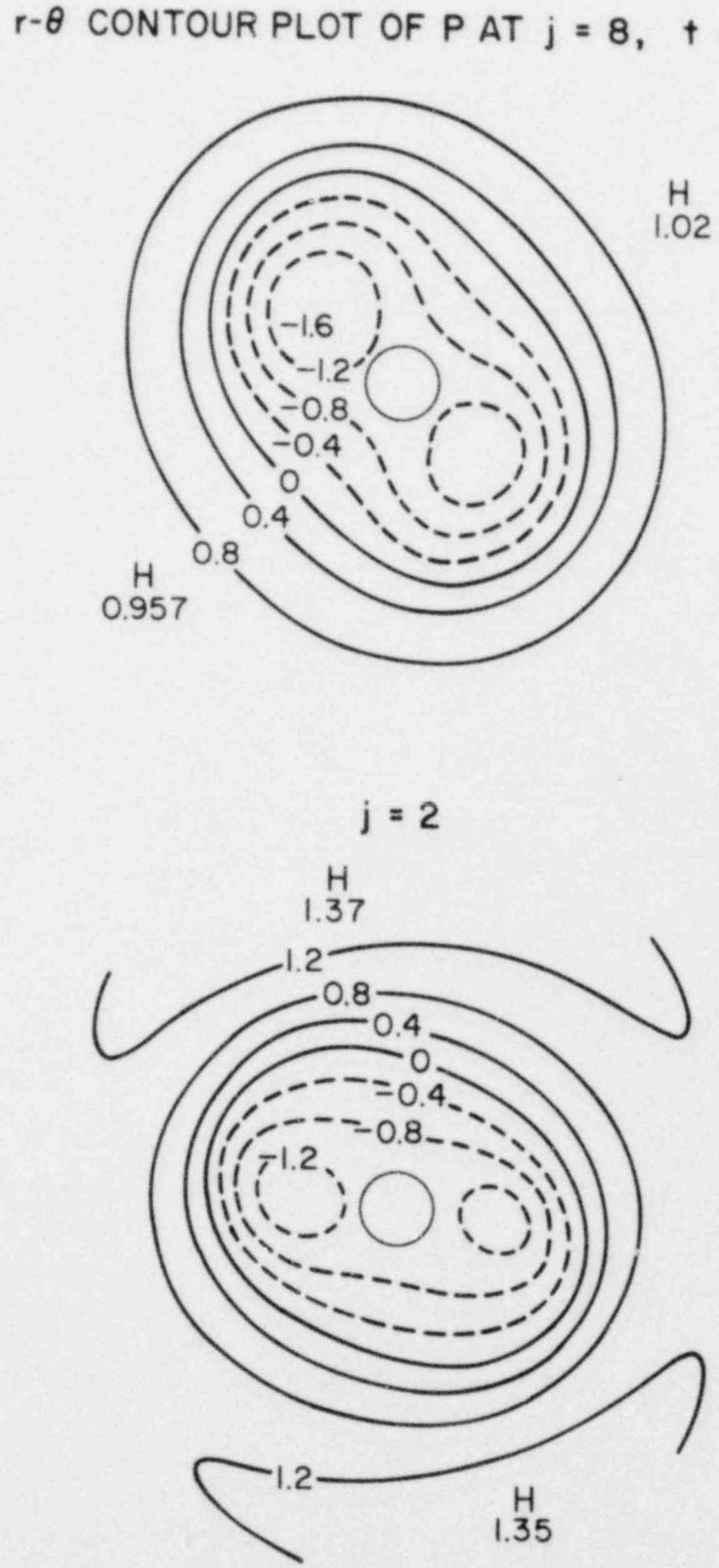

Fig. 6.7. Horizontal contour plots of P at j = 2 and j = 8 which illustrates that the pattern shifts clockwise with height.

Table 1

Total Energy vs. Time

t	E
0.0	2.250
10.0	6.912
20.0	6.897
30.0	7.184
40.0	8.159
50.0	8.183
60.0	8.175

The aximuthally averaged fields are changed in some respects by t = 60. The inner core region 'spun-up', the vertical velocity central minimum has lowered in position and the central pressure has reduced.

The total kinetic energy, viz

$$E(t) = \iiint_{\text{Volume}} \frac{u^2+v^2+w^2}{2} \, r \, dr \, d\theta \, dz$$

is tabulated (Table 1). After an initial increase, E levels of: and remains fairly constant until approximately t = 20: then increases rapidly until t = 40 and then holds constant as long as we continued the integration (t = 60). The increase in E corresponds to the time when the unstable waves are growing to finite amplitude. E becomes constant again when the finite amplitude waves have reached some sort of equilibrium and persist as long as the integration continues.

7.0 Interpretations

The first order of business is to demonstrate that the asymmetric wave structure may arise because the basic axisymmetric flow of the model is unstable. Recall the material derived in Section 4; first the Howard and Gupta criterion that the flow is necessarily stable to axisymmetric disturbances if

$$A \equiv \frac{1}{r^3} \frac{\partial \bar{\Gamma}^2}{\partial r} - \frac{1}{4} \left(\frac{\partial \bar{w}}{\partial r}\right)^2 > 0$$

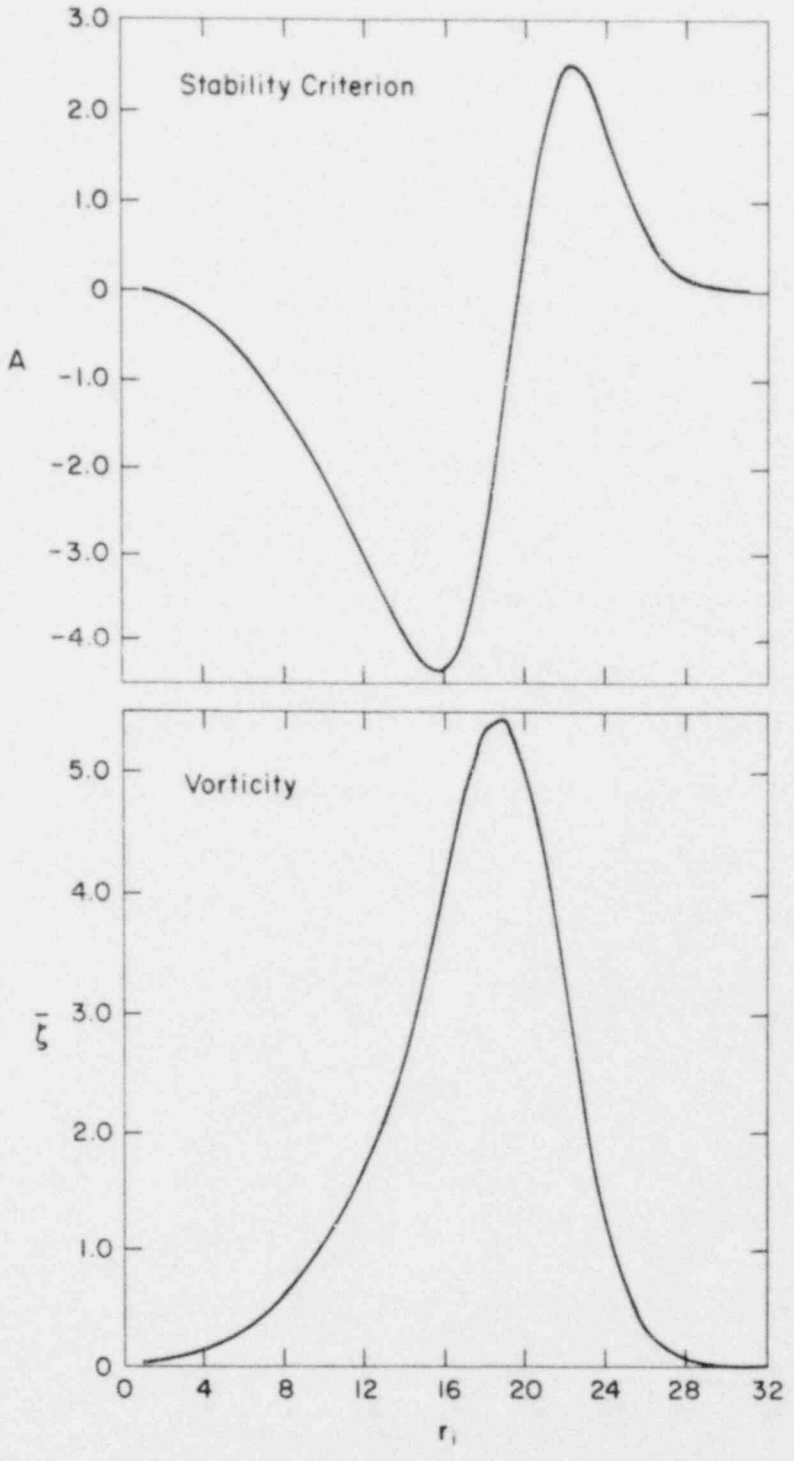

Fig. 7.1. The stability function A and the azimuthally averaged vorticity $\bar{\zeta}$ as a function of r at $z = 15\Delta z$.

and second that (for $\bar{w}$ = ct) the flow is stable to two-dimensional disturbances if the vorticity $\bar{\zeta}(r)$ is a monotonic function of r. Fig. 7.1 contains a graph of A and $\bar{\zeta}$ vs. r at z = 15Δz. (Recall that all stability analyses are, to our knowledge, for mean flows $\bar{\zeta}(r)$, $\bar{w}(r)$, which are independent of z, this is only approximately true in this case and probably most true near the midsection of our domain.)

What form does the instability take? Consider for a moment the classical Kelvin-Helmholtz instability of a parallel shear flow $\bar{U}(z)$. The basic vorticity vector is U_z into the page and thus perpendicular to the mean flow. As an unstable wave grows 'billows' tend to form along the vortex lines. Now consider an idealization of the flow in Fig. 6.2 a-d; the flow (Fig. 7.2) inside the inner ring is downward and has very little tangential component. The flow on the outer ring is strongly swirling and rising. If the flow is nearly cylindrical (i.e., $\partial/\partial z = 0$), the mean vorticity at the dashed ring is

$$\bar{\xi} = 0, \qquad \bar{\eta} = -\frac{\partial \bar{w}}{\partial r} < 0, \qquad \bar{\zeta} = \frac{1}{r}\frac{\partial \bar{\Gamma}}{\partial r} > 0$$

Thus, the vorticity vector points upward and in the negative azimuthal direction. If and when the flow depicted in Fig. 7.3 becomes unstable, we expect the vorticity to accumulate along the helical vortex lines of the basic flow in much the same way as it occurs in the Kelvin-Helmholtz problem. Fig. 7.3 displays an r-θ plot of the vertical vorticity for t = 60. The accumulation of vorticity at particular azimuths is evident. Further, the reason for the clockwise shift with height observed of the multiple vortex is now obvious.

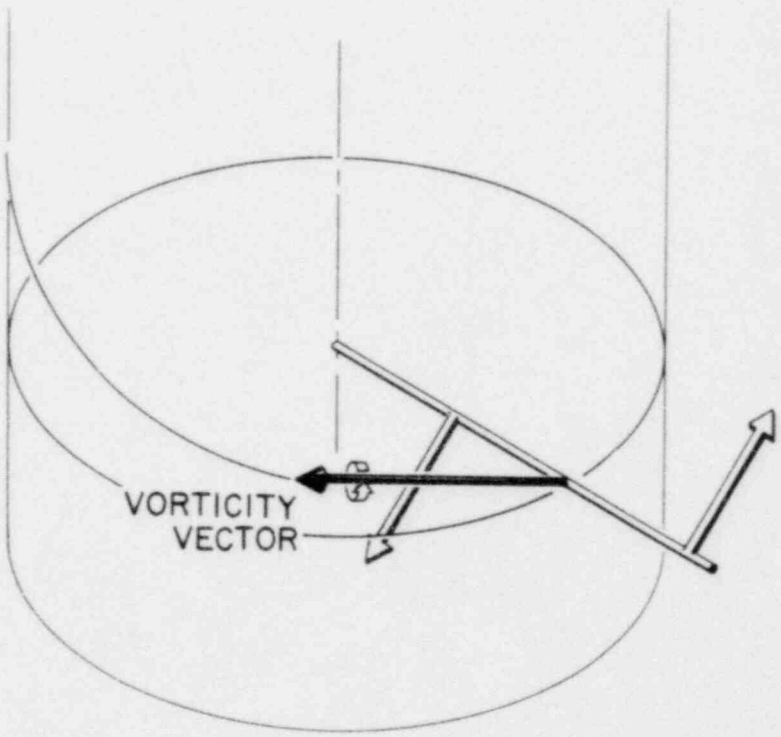

Fig. 7.2. Idealization of the vorticity vector of Fig. 6.2 a-d; the flow inside the ring is downward with very little tangential component. The flow outside the ring is strongly swirling and rising. Thus the vorticity vector points upward and in the negative azimuthally direction.

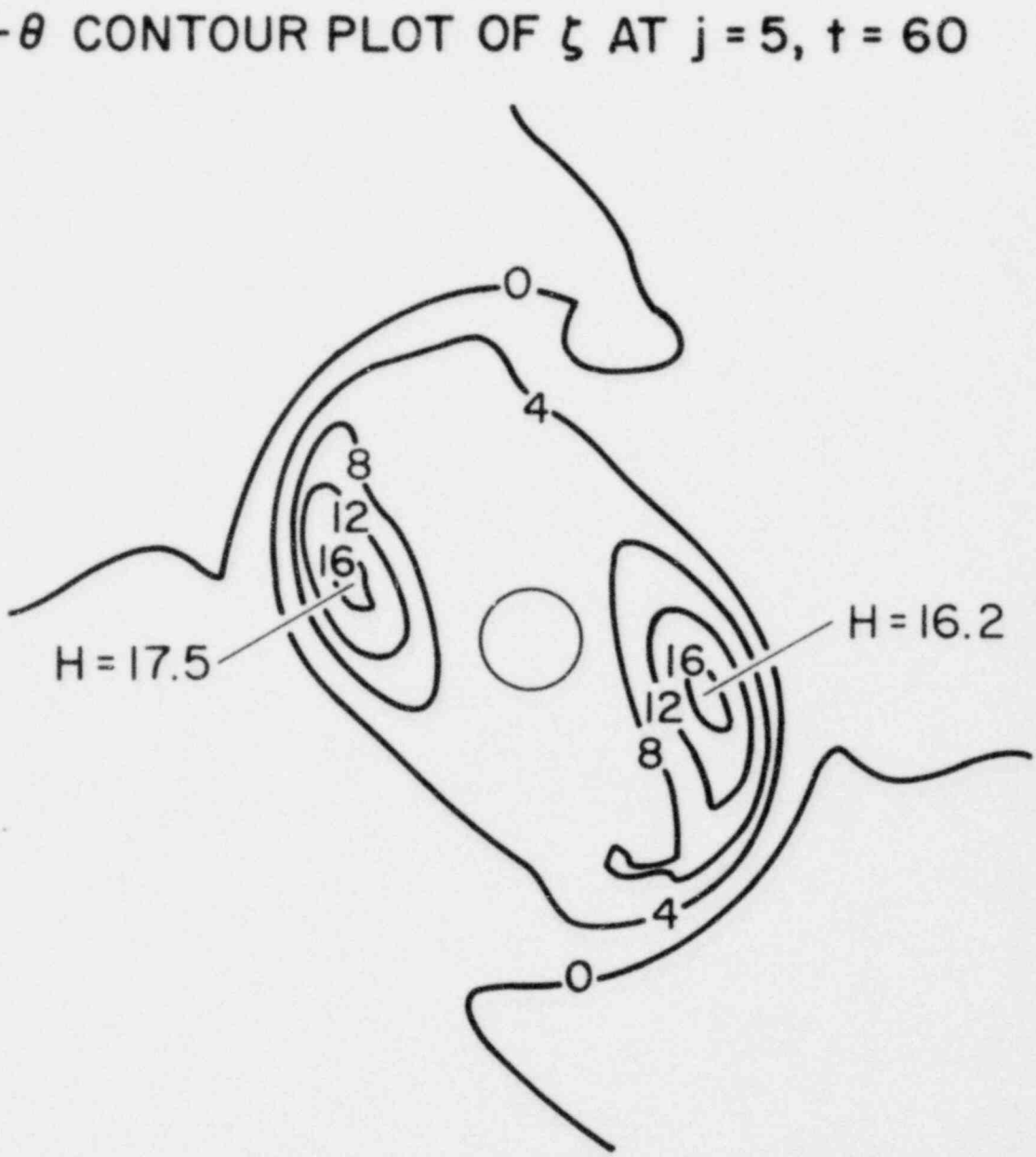

Fig. 7.3. mθ contour plot of the vertical vorticity at j = 5 and t = 60.

Near the top of the domain the vortex lines are bent to the horizontal because $u = v = 0$, thus $\zeta = (rv)_r/r - u_\theta/r = 0$.

Since we require $v = 0$ at $z = 2$, a 'boundary layer' forms because the interior flow has $v \neq 0$. Recall that $\xi = \frac{w_\theta}{r} - v_z$, thus, the large vertical graident of v ($v_z < 0$, $\xi > 0$) dominates the radial component of the vorticity. Hence, the large value of $\bar{v}$ near the top of the domain in Fig. 6.4c may be thought of as a consequence of the multiple vortex (near the lower surface) extending upward and over to the horizontal at $z = 2$. This pehnomenon is observed in the laboratory experiment described above (J.T. Snow, private communication).

That $\bar{v}(r, z, t)$ is increasing with time for small r, as the unstable wave grows suggests that the waves transport angular momentum inwards. This should be so according to a trivial extension of theorem by Held (1975). Consider a two-dimensional flow (r,θ) with mean vorticity $\bar{\zeta}(r)$; the equation governing the perturbations is

$$\zeta'_t + \frac{\bar{v}}{r}\zeta'_\theta = -u'\,\bar{\zeta}_r. \tag{7.1}$$

where

$$\zeta' = \frac{(r\psi'_r)_r}{r} + \frac{\psi'_{\theta\theta}}{r}; \qquad u' = \frac{-\psi'_\theta}{r}, \quad v' = \psi'_r$$

and ψ' is the perturbation streamfunction. Multiplying 7.1 by ζ' then averaging over θ obtains

$$\overline{u'\zeta'} = -\frac{\frac{\partial}{\partial t}\frac{\overline{\zeta'^2}}{2}}{\bar{\zeta}_r} \tag{7.2}$$

It is easy to show that

$$\overline{u'\zeta'} = \frac{1}{r^2}\left(r^2\,\overline{u'v'}\right)_r \tag{7.3}$$

Considering the mean azimuthal momentum equation (again in two-dimensions) obtains

$$\frac{\partial}{\partial t}\,\bar{v} = -\frac{1}{r^2}\,(r^2\,\overline{u'v'})_r \tag{7.4}$$

Combining (7.2)-(7.4) gives then

$$\frac{\partial}{\partial t}\,\bar{v} = \frac{\frac{\partial}{\partial t}\,\frac{\overline{\zeta'^2}}{2}}{\bar{\zeta}_r} \tag{7.5}$$

The numerator of the RHS of (7.5) is positive for a growing wave. As we see from Fig. 7.1, $\bar{\zeta}_r > 0$ over the entire inner part and accordingly $\bar{V}$ increases Of course, this analysis is restricted to two-dimensional flow but, nonetheless appears to give a reasonably accurate picture of the wave-mean flow interaction.

Finally, we must mention the increase in total energy which accompanies the transition to multiple vortices. Such an increase is, of course, not impossible since we have open system where energy may pass in and out. The energy equation is

$$\frac{\partial}{\partial t}\left(\frac{u^2+v^2+w^2}{2}\right) + \frac{1}{r}\frac{\partial}{\partial r}\,(ruH) + \frac{1}{r}\frac{\partial}{\partial \theta}\,(vH) + \frac{\partial}{\partial z}\,wH = Re^{-1}\,V\cdot\nabla^2 V \tag{7.6}$$

where $H = P + \frac{u^2+v^2+w^2}{2}$, the total head. Integrating 7.6 over the domain gives

$$\frac{\partial}{\partial t}\,E = -\underset{\substack{\text{inflow}\\ \text{boundary}}}{\iiint} uH\,d\theta dz - \underset{\substack{\text{outflow}\\ \text{boundary}}}{\iiint} wHrd\theta dz + \underset{\text{Volume}}{\iiint} \text{Dissipation} \tag{7.7}$$

H involves u, v, w and P and we specify conditions on the derivatives of w and P at inflow and outflow (so w and P may change). Our calculations indicate that the presence of the multiple vortex does not allow the energy to pass out as quickly as it enters thus accumulation occurs until a balance between energy flux divergence and dissipation is reached.

Due to limitations of computer time only a restricted combination of parameters could be studies; the cases studies are summarized in Appendix I. Inlcuded also are some statistics such as the amplification factor ($- v_{max}/v_R$) and the radius of maximum winds from the domain center (r_{max}) and the azimuthal average amplification factor $\bar{v}_{max}/v_R$.

8.0 Conclusions

We believe we've achieved the first successful simulation of the multiple vortex phenomenon. The highly asymmetric nature of the multiple vortex has precluded analytical descriptions heretofore; however, now a model based on exact solutions of the Navier-Stokes equations exists.

The model indicates that in a horizontal cross-section the circulation is centered on a strong gradient of the vertical velocity with the maximum tangential velocity on the side of maximum vertical velocity. The core of this asymmetric vortex shifts clockwise with height (the mean streamlines of the parent vortex are counter-clockwise). The peak tangential velocity associated with the multiple vortice was found to be 20%-30% greater than either the azimuthally averaged larger scale flow or that obtained in an equivalent axisymmetric model.

ACKNOWLEDGMENT

Acknowledgment is made to the National Center for Atmospheric Research, which is sponsored by the National Science Foundation for computer time used in this research. Dr. Robert F. Abbey, Jr. was the NRC technical monitor.

APPENDIX I

Other Cases

Case	S	R_e	K	$\bar{v}_{max}/v_R$	v_{max}/v_R	r_{max}	z_{max}	Remarks
1	1	150	∞	1.7	2.05	.44	0	This case studied in detail in § 6.7
2	1.5	150	∞	1.6	2.06	.62	0	Initially, 4 MVs appear, later only 2 dominate
3	2	150	∞	1.4	1.95	.78	0	Initially, 4 MVs appear, later 2 dominate with 2 other weaker MVs present.
4	1	150	1.	1.6	2.0	.55	.3	Vertical velocity some stronger at low levels.
5	1	300	1.	1.76	2.4	Variable, Variable		2 MVs present with 1 much stronger than the other
6	4	150	1.	1.14	1.5	Variable, Variable		4 MVs
7	4	100	1.	1.11	1.5	Variable, Variable		4 MVs

REFERENCES

Batchelor, G. K., and A. E. Gill, 1962: Analysis of the stability of axisymmetric jets. J. Fluid Mech., 14, 529-551.

Bergman, K. H., 1969: On the dynamic stability of convective atmospheric vortices. Ph.D. Dissertation, Univ. of Washington, 170 pp.

Brooks, E. M., 1949: The tornado cyclone. Weatherwise, 2, 32-33.

Browning, K. A., 1965: Some inferences about the updraft within a severe local storm. J. Atmos. Sci., 20, 533-545.

_____, and F. Ludlam, 1962: Airflow in convective storms. Quart. J. Roy. Meteor. Soc., 88, 117-135.

Brandes, E. A., 1978: Mesocyclone evolution and tornadogenesis: some observations. Mon. Wea. Rev., 106, 995-1011.

Church, C. R., J. T. Snow, G. L. Baker, and E. M. Agee, 1979: Characteristics of tornado-like vortices as a function of swirl ratio: a laboratory investigation. J. Atmos. Sci., 36, 1755-1776.

Davies-Jones, R. P., 1973: The dependence of core radius on swirl ratio in a tornado simulation. J. Atmos. Sci., 30, 1427-1430.

Forbes, G. S., 1978: Three scales of motion associated with tornadoes. Final Report to U.S. Nuclear Regulatory Commission, (NUREG/CR-0363 RB, 359 pp.*

Fujita, T. T., 1970: The Lubbock tornadoes: a study of suction spots. Weatherwise, 23, 160-173.

_____, 1976: History of suction vortices. Proc. of the Symposium on Tornadoes, Texas Tech Univ., 28-88.

*Available for purchase from the National Technical Information Service, Springfield, VA 22161.

Golden, J. H., and D. Purcell, 1977: Photogrammetric velocities for the Great Bend, Kansas, torna o of 30 August 1974: Accelerations and asymmetries. Mon. Wea. Rev., 105, 485-492.

Held, I. M., 1975: Momentum transports by quasi-geostrophic eddies. J. Atmos. Sci., 32, 1494-1497.

Howard, L. M., and A. S. Gupta, 1962: On the hydrodynamic and hydromagnetic stability of swirling flows. J. Fluid Mech., 14, 463-476.

Kelvin, J. T., 1880: On the vibrations of a columnar vortex. Philosophical Magazine, 10, p. 155.

Kuo, H.-L., 1967: Note on the similarity solutions of the vortex equations in an unstably stratified atmosphere. J. Atmos. Sci., 24, 95-97.

Lamb, H., 1932: Hydrodynamics, Dover Publications, 738 pp.

Lemon, L. R., and C. A. Doswell, 1979: Severe thunderstorm evolution and mesocyclone structure as related to tornadogenesis. Mon. Wea. Rev., 107, 1184-1197.

Lewellen, W. S., 1971: A review of confined vortex flows. NASA Rep. CR-177w, 219 pp.

_____, 1976: Theoretical models of the tornado vortex. Preprints, Symposium on Tornadoes, Texas Tech Univ., 107-144.

_____, and M. E. Teske, 1977: Turbulent transport model of low level winds in a tornado. Preprints 10th Conference on Severe Local Storms, Omaha, Amer. Meteor Soc., 291-298.

Rayleigh, J. W. S., 1892: On the question of stability of the flow of fluids. Philosophical Magazine, 34, 59.

_____, 1916: On the dynamics of revolving fluids. Proc. Roy. Soc. of London A, 43, 148-154.

Rotunno, R., 1977: Numerical simulation of a laboratory vortex. J. Atmos. Sci., 34, 1942-1956.

_____, 1978: A note on the stability of a cylindrical vortex sheet. J. Fluid Mech., 87, 761-771.

_____, 1979: A study on tornado-like vortex dynamics. J. Atmos. Sci., 36, 140-155.

_____, 1980: Dynamics of a convective swirling boundary layer. J. Fluid Mech., 97, 623-670.

_____, 1981: On the evolution of thunderstorm rotation. To appear in Mon. Wea. Rev.

Snow, J. T., 1978: On inertial instability as related to the multiple vortex phenomenon. J. Atmos. Sci., 35, 1660-1671.

Stout, G. E., and F. A. Huff, 1953: Radar records Illinois tornadogenesis. Bull. Amer. Meteor. Soc., 34, 281-284.

Sullivan, R. D., 1959: A two-cell solution of the Navier-Stokes equations. J. Aero. Sci., 26, 767-768.

Swarztrauber, P., and R. Sweet, 1975: Efficient FORTRAN subprograms for the solution of the Elliptic Partial Differential Equations. NCAR Tech. Note NCAR-TN/IA-109, 139 pp.

Ward, N. B., 1972: The exp'anation of certain features of tornado dynamics using a laboratory model. J. Atmos. Sci., 49, 1194-1204.

Williams, G. P., 1969: Numerical integration of the three-dimensional Navier-Stokes equations for incompressible flow. J. Fluid. Mech., 37, 727-750.

NRC FORM 335 (7-77)

U.S. NUCLEAR REGULATORY COMMISSION

BIBLIOGRAPHIC DATA SHEET

1. REPORT NUMBER (Assigned by DDC)
NUREG/CR-1840

4. TITLE AND SUBTITLE (Add Volume No., if appropriate)
A Numerical Model Pertaining to the Multiple Vortex Phenomenon

2. (Leave blank)

3. RECIPIENT'S ACCESSION NO.

7. AUTHOR(S)
R. Rotunno and D. K. Lilly

5. DATE REPORT COMPLETED
MONTH: November YEAR: 1980

9. PERFORMING ORGANIZATION NAME AND MAILING ADDRESS (Include Zip Code)
Cooperative Institute for Research in the Environmental Sciences
University of Colorado
Boulder, CO 80303

National Center for Atmospheric Research
Boulder, CO 80303

DATE REPORT ISSUED
MONTH: January YEAR: 1981

6. (Leave blank)

8. (Leave blank)

12. SPONSORING ORGANIZATION NAME AND MAILING ADDRESS (Include Zip Code)
Division of Reactor Safety Research
Office of Nuclear Regulatory Research
U.S. Nuclear Regulatory Commission
Washington, D.C. 20555

10. PROJECT/TASK/WORK UNIT NO.

11. CONTRACT NO.
NRC-04-78-247
FIN B6238

13. TYPE OF REPORT
Final report

PERIOD COVERED (Inclusive dates)
May 1, 1978 - April 30, 1980

15. SUPPLEMENTARY NOTES

14. (Leave blank)

16. ABSTRACT (200 words or less)

A three dimensional numerical model has been constructed for study of the multiple vortex phenomena. It is found that highly asymmetric vortices form at the core boundary of the larger parent vortex for certain values of the swirl ratio, S and radial Reynolds number. The asymmetric vortices arise as an instability of the initially axisymmetric parent vortex. The peak velocity associated with the mature asymmetric vortices can be 20%-30% larger than that of the parent vortex. The asymmetric vortices assume the form of intertwining helicies of negative pitch angle (the streamlines of the parent vortex are helical with positive pitch angle). This and other features are in agreement with a relevant laboratory experiment.

17. KEY WORDS AND DOCUMENT ANALYSIS

17a. DESCRIPTORS

17b. IDENTIFIERS/OPEN-ENDED TERMS

18. AVAILABILITY STATEMENT
Unlimited

19. SECURITY CLASS (This report)
Unlimited

21. NO. OF PAGES

20. SECURITY CLASS (This page)
Unlimited

22. PRICE
$

NRC FORM 335 (7-77)